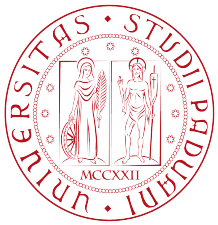

UNIVERSITÀ DEGLI STUDI DI PADOVA

Dipartimento di Matematica "Tullio-Levi Civita"

UNIVERSITÉ PARIS-DAUPHINE PSL

Département de Mathématiques et Applications

Master Degree Course in Mathematics

Double Degree Course "MAPPA"

MOVING BOUNDARY PROCESSES WITH APPLICATIONS: MATHEMATICAL ANALYSIS OF CORAL'S GROWTH

Advisor:

Prof. Emmanuel Dormy

Student:

Mauro D'Annibale

2017357 / 22100578

Co-Advisor:

Prof. Mario Putti

Project coordinator:

Prof. Francesco Rossi

Academic year 2021/2022

Acknowledgements

I would like to acknowledge my Advisor, Prof. Emmanuel Dormy, and co-Advisor, Prof. Mario Putti, for guiding me throughout this project. I acknowledge moreover Prof. Ludivine Oruba and the *SWAG* project for the support in this internship.
I really thank all the Academic Institutions that have supported and hosted me during these two years of master in Padova and Paris.

UNIVERSITÀ DEGLI STUDI DI PADOVA

Dauphine | PSL
UNIVERSITÉ PARIS

| PSL

SORBONNE UNIVERSITÉ

Contents

General introduction **1**

1 Moving-boundary processes **4**

1.1 Mathematical description: Conformal maps 4

1.1.1 Laplacian Growth and Surface tension 6

1.2 Growth model in radial geometry 7

1.3 Diffusion-Limited aggregation 10

2 Instability **13**

2.1 Mullins-Sekerka instability on a circle 13

2.1.1 Numerical visualization withouth surface tension 16

2.1.2 Numerical visualization with surface tension 19

2.2 Mullins-Sekerka instability on a sphere 24

2.2.1 Spherical Harmonics 24

2.2.2 Stability analysis 26

3 Coral's growth simulation **30**

3.1 Laplacian growth in 2D 30

3.2 Fluid flow effect 33

4 Future perspectives **38**

Appendices

A PDEs tools **41**

A.1 Linear functionals and bilinear forms:
Lax-Milgram Theorem 41

A.2 Poisson equation 43

A.3 Stokes equation 44

A.3.1 Penalty method 45

A.4 Navier-Stokes Equation 45

A.5 Finite Element Method 49

A.5.1 Abastract formulation of the FEM for elliptic equations 49

B Random Walk **54**

B.1 Simmetric Random Walk and Diffusion Processes 54

C Codes **58**

C.1 Mullin-Sekerka's Instability 58

C.2 2D Coral's Growth 61

Bibliography **66**

Acknowledgements **68**

General Introduction

In this thesis we want to study numerically and mathematically the PDE system governing coral's growth. A few numerical models have already been introduced in computational sciences, but these are often discrete models and are not currently properly written in the PDE framework. Here we want to provide a mathematical and numerical analysis of the fingering instability responsible for coral branching and governing coral's growth. This general field is of significant importance in current ecology because corals are currently threatened by the current increase of the sea surface temperature as well as by other antropic perturbations. Understanding how fast coral can recover (a mechanism known as resilience) is thus an essential issue in ecology. More generally the understanding of morphogenesis, the generation of shape, is a fundamental and fascinating problem in biology.

Many of the patterns that can be observed in nature or in experiments are the result of surface instabilities. These structures typically arise when an interface is forced to move due to fluxes of heat and/or mass or because of a mechanical forcing that leads to a pressure gradient. A small perturbation of the moving boundary will either grow unstably or decay such that the boundary recovers its original shape. The stability of such a perturbation is determined both by the geometry of the surface and by the governing PDE equations.

If the conditions are such that the moving boundary is unstable, it will evolve into some kind of a pattern. The characteristics and morphology of the final structure will also depend on the parameters that determine the stability of the interface. Branching occurs in many physical systems, such as crystallisation, aggregation, electrical discharge and viscous fingering. We want to focus in this thesis on the particular case of coral's growth.

If the nutriment diffuse very efficiently, the concentration of nutriment will be governed by the Laplace equation. Such problems belong to an important category of surface evolution processes called Laplacian growth problems. In such problems, the interface velocity is a function of the gradient of nutriments. Laplacian growth is viewed as a fundamental model for pattern formation. In Laplacian growth, the displacement of an interface $\vec{\gamma}$ is governed by a field of some quantity C which satisfies the Laplace equation

$$\Delta C = 0.$$

The quantity C could correspond to some pressure field, electric field or a growth resource. In the case of coral's growth it models a density of nutriments. The displacement of the interface is then given by

$$\partial_t \vec{\gamma} = \vec{\nabla} C(\vec{\gamma}).$$

This indicates that the local displacement of the interface is proportional to the gradient of the field. As we mentioned before, central to understanding the mechanism of branching in Laplacian growth is the so-called Mullins-Sekerka instability; as soon as a tiny bump of the interface appears, the gradient of the surround field at the bump will be slightly larger than elsewhere. Hence, an instability occurs, locally the growth is enhanced, enlarging the initial perturbation. In such instabilities the presence or not of the surface tension in the model is fundamental. Indeed the presence of the surface tension in such models allows to control the high frequency modes, which are the most unstable.

A fascinating example of such Laplacian growth is the study of coral's growth. The situation is however more complex, as polyps size will limit high frequency modes, rather than surface tension. Also, while coral growth can at first be mathematically investigated in a fluid at rest, in practice corals usually develop in a flow of water. It is believed that the pattern of coral colonies is strongly influenced by the effect of the fluid flow. The governing PDE for the flow is then the Navier-Stokes (NS) equation

$$\rho \frac{\partial \vec{u}}{\partial t} - \nabla \cdot [\eta(\nabla \vec{u} + \nabla \vec{u}^T)] + \rho(\vec{u} \cdot \nabla)\vec{u} + \nabla p = F,$$

$$\nabla \cdot \vec{u} = 0.$$

The solution of the NS equations can be approached numerically. Analytical solutions can also be sought in local cases (boundary layers). Then the concentration of nutriment can be obtained via an advection-diffusion equation

$$\frac{\partial C}{\partial t} + \vec{u} \cdot \nabla C = D\Delta C,$$

where C is the nutriment concentration, $\vec{u}$ is the velocity field obtained from the NS equations and D is some diffusion coefficient. Notice that, since the time's growth of a coral is very slow, one can use the steady version of the previous PDEs, i.e. the stationary case. With these informations one can then perform the accretion step (growth) of the coral. Different techniques have already been tested, usually discrete in essence (i.e. not following the discretisation of a PDE), such as for example by Kaandrop *et al.* ([4]). In such models, the thickness of the deposited layer was determined by a set of arbitrary functions, known as "growth functions", which returned local measurements of the current growth form and of a simulated environment of the organism. Each of the branches contained an explicit growth axis, whose direction governed the growth of the branch. Through one of the growth functions, the angle between the coral surface and the growth axis determined the thickness of the branch, thus generating a rod shaped branching.

In this thesis we want to revisit this computational approach with a PDE formalism and infer the parameters that control coral branching (not all coral have branches, some grow with a nearly spherical shape).

Chapter 1

Moving-boundary processes

Many of the patterns observed in nature can be described in terms of a surface that is moving due to external transport processes and properties of the surface itself. In the most simple examples, this external transport process can be described by a scalar field which satisfies the diffusion or Laplace equation. The whole boundary is moving due to gradients in this field, whereas a particular pattern is formed only if some of the impurities on the surface are unstable. The kinetics of the moving boundary are also sensitive to such impurities, and play an important role for the resulting pattern.

1.1 Mathematical description: Conformal maps

The two-dimensional mathematical description is convenient to work with and easy to visualize. In particular, complex analysis can be applied: the close resemblence between complex function theory and geometrical shapes is the key to the usefulness of complex numbers for these purposes. In complex analysis, a function $g(z) = \omega = u(x, y) + iv(x, y)$ involves a correspondance between the four variables x, y, u, v, and the conventional graphing procedure can not be used. To avoid this inconvenience, graphing in complex analysis is rather done using two planes: the z-plane and the ω-plane. If the mapping $\omega = g(z)$ preserves angles, it belongs to a family called *conformal maps*. More precisely, a map that is conformal at z_0 preserves the size and orientation of the angle between any two curves through z_0. It is well known that if $g(z)$ is analytic in a domain D,

then $g(z)$ is conformal at every point in D where its first derivative is not equal to zero. Moreover if a mapping is conformal at a point z_0, then it has a local inverse there. Most applications of conformal mapping involve harmonic functions, which are solutions to Laplace's equation,

$$\Delta\phi = 0.$$

From the Cauchy-Riemann equations, it is easy to show that the real and imaginary parts of an analytic function are harmonic, but the converse is also true: every harmonic function is the real part of an analytic function, $\phi = \mathrm{Re}\,\Phi$, the *complex potential*. This connection easily produces new solutions to Laplace's equation in different geometries. Suppose that we know the solution, $\phi = \mathrm{Re}\,\Phi$, in a simply connected domain in the ω-plane, Ω_ω, which can be reached by conformal mapping, $\omega = f(z,t)$, from another, possibly time dependent domain in the z-plane, $\Omega_z(t)$. A solution in $\Omega_z(t)$ is then given by

$$\phi(z,t) = \mathrm{Re}\,\Phi(\omega) = \mathrm{Re}\,\Phi(f(z,t)), \tag{1.1}$$

because $\Phi(f(z))$ is also analytic, with a harmonic real part. In other words: if a domain can be reached by a conformal map of another domain, then a function that is harmonic in one of the domains automatically must be harmonic in both domains. The only restriction to take care of when mapping harmonic functions between different domains, is that the boundary conditions must also be conformally invariant. This is true for Dirichlet ($\phi = \text{const}$) or Neumann ($\mathbf{n} \cdot \nabla\phi = 0$) boundary conditions. Most other boundary conditions invalidate Eq. (1.1) and thus complicate the analysis.

The usefulness of conformal maps becomes even more evident when introducing further properties: The *Riemann mapping Theorem* states that for any simply connected domain D in the z-plane, which is not the entire z-plane, there exists a unique conformal map $\omega = g(z)$ that brings D onto the unit disc, and that transforms the boundary of D into the unit circle. Even though not stated explicitly, the Riemann mapping Theorem guarantees the existence of a unique conformal mapping between any two simply connected domains. As a consequence, one is not restricted to the unit disc or the physical plane when dealing with Laplacian fields. When working with a problem that is described by an harmonic function, the treatment may be complicated if its geometry is inconvenient in the physical plane. If it is possible to find a domain where the geometry of the problem makes it

simpler to solve, then the Riemann mapping theorem guarantees that there will be a conformal map that can take the harmonic function there. If there exists a conformal mapping of D_1 onto D_2, then D_1 and D_2 are said to be conformally equivalent. That is, the conformal mapping between the two must satisfy the usual axioms of an equivalence relation: reflexivity, symmetry and transitivity. The transitive property implies that the composition of two conformal mappings is also a conformal mapping. This property turns out to be especially useful when dealing with moving boundaries and pattern forming precesses.

When applying conformal maps to moving boundaries, growing domains and pattern forming processes, the idea goes like this: a reference domain is chosen in such a way that the problem at hand is nice to handle in that geometry. Examples of reference domains are the unit disc, the exterior of the unit circle, or the upper half-plane. Then the conformal map between the domain D in physical space (say z-plane) and the reference domain (which lies in the mathematical ω-plane) is found. Now the evolution of D can be studied by mapping it to R, imposing controlled changes there, and then applying the inverse map back to the z-plane to study what the real effects of the changes will be in the physical space. As an example, let $\omega = g(z)$ be the mapping of D onto R, and let $f(\omega)$ be its inverse. If $h(\omega)$ represent a small perturbation or growth of R, then $f(h(\omega))$ is the composition of mappings that codes for how these changes affect the domain in the z-plane. Another technique uses instead a fixed reference domain. This requires that the mapping $g(z)$ and hence also $f(\omega)$ must change whenever the structure in the z-plane changes. Both techniques have their positive and negative sides, and there is typically a certain range of moving-boundary processes for which each of them is particularly useful.

1.1.1 Laplacian Growth and Surface tension

As already anticipated, the Laplacian growth model assumes that the normal velocity of the interface, v_n, is proportional to the field gradient at the interface to some exponent η:

$$v_n \sim |\nabla U|^{\eta}, \tag{1.2}$$

where U is a Laplacian field that can represent pressure, temperature, concentration, or some other quantity, depending on the problem studied. If one assumes zero surface

tension, the boundary condition at the interface is conformally invariant and confromal mapping tecniques can be used to solve that problem. *Surface tension* is introduced by the boundary condition $U(z_b) = \gamma_\kappa$ for the points z_b at the interface. This boundary condition is *not* conformally invariant, which compilcates the analysis considerably. Surface tension is very significant in case of high curvature; the growth velocity around thin fingers will therefore be very high, and surface tension is the only *stabilising force* that can oppose the rapid growth of the parts of the interface with high curvature. This concept will be well studied in Chapter 2.

1.2 Growth model in radial geometry

A radial growth problem is convenient to work with as it is fairly simple to handle analytically when using complex analysis. The following model considers Laplacian growth of a nearly circular domain in the absence of surface tension. If a perfectly circular domain is growing in a harmonic field U with an equally large gradient at all points of the domain boundary, then the boundary will grow equally fast at all points and hence the circular shape will be preserved. This is not a very relevant example to study because nature itself never provides anything that is perfectly circular. A seemingly circular inlet in viscous fingering will, in practice, provide an initial influx which is not exactly the same in all directions. This leads to a starting configuration for the pattern evolution which is only nearly circular. The model considers a nearly circular domain; more precisely, the unit circle is perturbed by a function $h(\theta) = \varepsilon \cos(m\theta)$, introducing m protuberances of amplitude ε around the rim of the unit disc. This is exactly the same starting configuration as for the Mullins-Sekerka instability analysis in Section 2.1. We want to study how the boundary of this nearly circular domain will evolve in time when it is growing in a Laplacian field U. For semplicity, surface tension is not included in the model, hence we will use the conformally invariant boundary condition $U(z_b) = 0$ for all point z_b at the interface of the growing domain, which allows us the use of conformal mapping techniques. The evolution of the boundary is dependent on the Laplacian field between the boundary and infinity, hence this will be the region where the Laplace equation needs to be solved. In [2] a conformal map $z = f(\omega) = \omega + \varepsilon\omega^{1-m}$ from the

complement of the unit disc onto the exterior of a slightly distorted unit circle is derived. In order to study the evolution of the boundary $r(\theta) = 1+h(\theta)$ of the perturbed domain with respect to the unit circle, a dynamical equation for $f(\omega)$ is needed. We introduce $\alpha(t)$ and $\beta(t)$ in the following way:

$$f(\omega,t) = \alpha(t)\,\omega + \beta(t)\,\varepsilon\,\omega^{1-m} \tag{1.3}$$

with initial conditions $\alpha(0) = 1$ and $\beta(0) = \varepsilon$.
Every harmonc function $\mathcal{U}(z)$ can be written as the real part of an analytic function: $\mathcal{U}(z) = \mathrm{Re}\,\mathcal{V}(z)$, where $\mathcal{V}(x+iy) = \mathcal{U}(x,y) + i\mathcal{W}(x,y)$. Using the Cauchy-Riemann equations (since $\mathcal{V}$ is analytic) we can relate the complex potential to the field gradient, i.e.,

$$\nabla_z\mathcal{U}(z) = \frac{\partial\mathcal{U}}{\partial x} + i\frac{\partial\mathcal{U}}{\partial y} = \frac{\partial\mathcal{U}}{\partial x} - i\frac{\partial\mathcal{W}}{\partial x} = \left(\frac{\partial\mathcal{V}}{\partial x}\right)^* = \left(\frac{\partial\mathcal{V}}{\partial z}\right)^*, \tag{1.4}$$

in which the asterix denotes the complex conjugate.
In the exterior of the unit circle, the complex potential will be of the form $\mathcal{V}(\omega) = \log(\omega)$, which leads to $\mathcal{V}(z) = \log(f^{-1}(z,t))$ in the z-plane. The normal boundary velocity v_n in the z-plane may then be related to the mapping $f(\omega,t)$ through (1.2). Using $\eta = 1$, the result is

$$v_n \sim \left(\frac{\partial\mathcal{V}}{\partial z}\right)^* = \frac{1}{\omega^*\,f'(\omega,t)^*}, \tag{1.5}$$

where $f'(\omega,t) = \frac{\partial f}{\partial\omega}$. Another expression for the velocity of the surface is found from the time derivative of the mapping $z = f(\omega,t)$:

$$v_n = \frac{d}{dt}f(\omega,t) = \frac{\partial f}{\partial t} + \frac{\partial f}{\partial\omega}\frac{\partial\omega}{\partial\theta}\frac{\partial\theta}{\partial t}.$$

These two equations for v_n together give the dynamical equation for the map:

$$\omega^*\frac{\partial f^*}{\partial\omega}\frac{\partial f}{\partial t} + i\left|\omega\frac{\partial f}{\partial\omega}\right|^2\frac{\partial\theta}{\partial t} = 1,$$

hence,

$$\mathrm{Re}\left(\omega^*\frac{\partial f^*}{\partial\omega}\frac{\partial f}{\partial t}\right) = 1. \tag{1.6}$$

By inserting Eq. (1.3) in (1.6), a set of differential equations for $\alpha(t)$ and $\beta(t)$ are found:

$$\frac{d\alpha}{dt} = \frac{\alpha(t)}{\alpha^2(t) - (m-1)^2\,\beta^2(t)} \tag{1.7}$$

$$\frac{d\beta}{dt} = \frac{(m-1)\beta(t)}{\alpha^2(t) - (m-1)^2\,\beta^2(t)}. \tag{1.8}$$

In this way, solving this system of ODEs numerically, we obatined an analytical expression of the boundary evolutions.

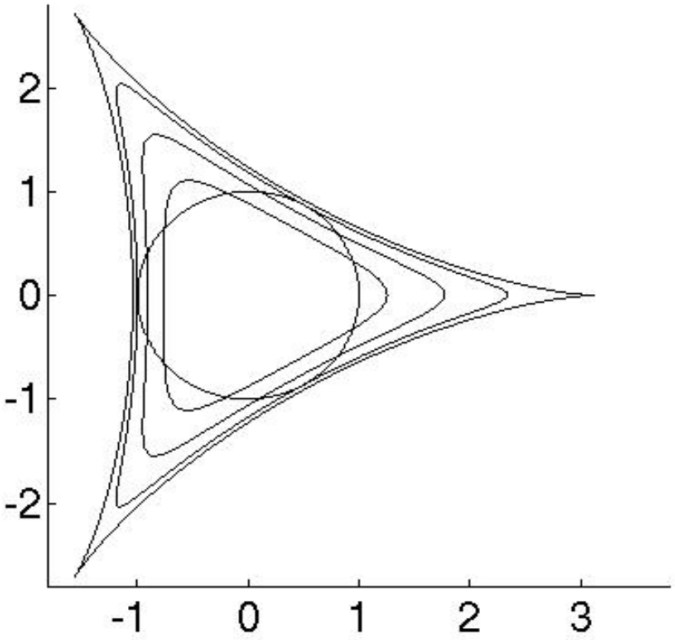

Figure 1.1: Evolution of a perturbed cirle leading to cusp singularities in finite time, [2]

The evolution of finite-time singularities from the unit circle, obtained by numerical integration of the Eqs. (1.7) -(1.8), for m = 3 and initial conditions $\alpha(0) = 1$ and $\beta(0) = 0.008$ can be seen in Figure 1.1.

Remark 1.2.1. Surface tension can also be incorporated into numerical simulations based on the same conformal-mapping formalism, which show how cusps are avoided by the formation of new fingers. That aspect will be explained in Section 2.1.1.

1.3 Diffusion-Limited aggregation

Diffusion-Limited Aggregation (DLA) was first introduced by Tom Witten and Len Sander in 1981 as a model for random, irreversible aggregation, although they and others quickly realized that the model is very widely applicable.
To understand the basics, consider colloidal particles undergoing Brownian motion in some fluid, and let them adhere irreversibly on contact with one another. Suppose further that the density of the colloidal particles is quite low, so one might imagine that the aggregation process occurs one particle at a time. We are then led to the following model. Fix a seed particle at the origin of some coordinate system. Now introduce another particle at a large distance from the seed, and let it perform a random walk. That second particle will either escape to infinity or contact the seed, to which it will stick irreversibly. Now introduce a third particle into the system and allow it to walk randomly until it either sticks to the two-particle cluster or escape to infinity. Clearly this process can be repeated. This algorithm leads to highly branched clusters with fractal structure. The fractal property arises because the tips shield the other parts of the cluster from incoming particles, and are therefore hit more often and hence grow faster than the inner parts of the stucture. It is quite remarkable that there is a huge similarity between DLA and Laplacian Growth processes. Indeed, since the particles are realised one by one and may take arbitrarly long time to hit the cluster, the probability density of the randomly walking particle is quasi-stationary and in the complement of the cluster satisfies the Laplace equation, with the cluster's surface providing a surface of constant probability density. In this case, the *probability of growth* (not the growth rate) at the surface is given by the gradient of this probability density. Thus DLA can be seen as a stochastic version of the Laplacian Growth Process. For a depper explanation of the connection between random walk and Laplace equation one can see Appendix B. The main difference between these two models is that Laplacian growth without surface tension is ill-posed, as we have seen in Sec. 1.2: the interface is unstable and evolves into singular cusps within finite time. Surface tension or some other regularising effect needs to be introduced in order to control singularities and keep the boundary stable (a more detailed explanation of this behaviour will be clarified in Chapter 2). In DLA, by contrast, the finite particle size prevents the appearance of any such singularities. The

important differences between the problems stem from the fact that Laplacian Patterns are grown layer by layer, whereas DLA is grown particle by particle.

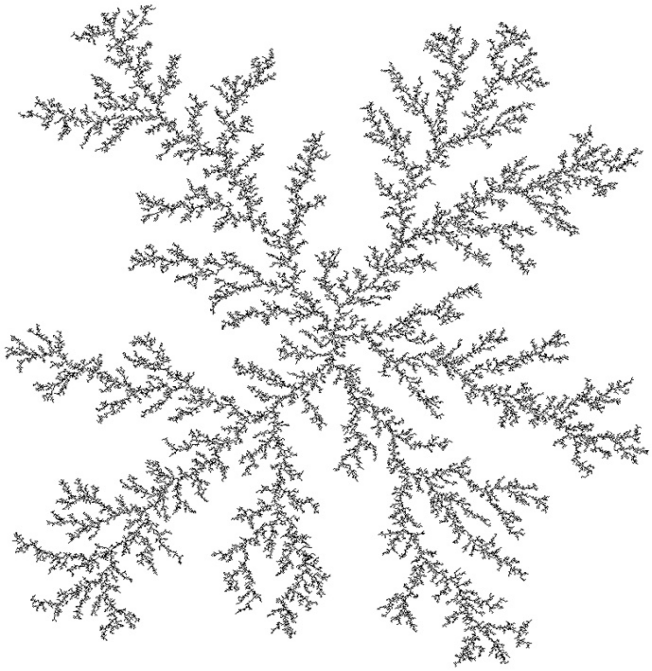

Figure 1.2: Example of DLA with a point attractor, [5]

In Figure 1.2 one can see a typical example of DLA with a point attractor, i.e. the procedure start with a single point at the center of the image. Of course others simulations can be done, using as attractor a whole line at the bottom where the new points enter form the top (Figure 1.3), or using a box attractor where new points enter in the interior (Figure 1.4). There are a number of ways of adding colour, Figure 1.5 has a circular seed region (toroidal bounds) and the particles are coloured by the order in which they were introduced. A huge variety of examples can be presented, either in 2D and in 3D. For further informations and simulations one can see [5] - [6].

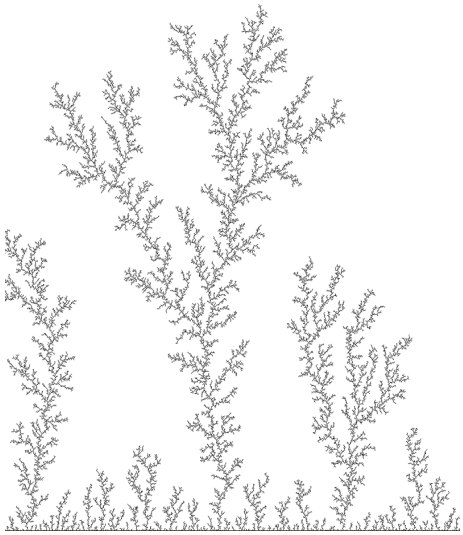

Figure 1.3: Line attractor, [5]

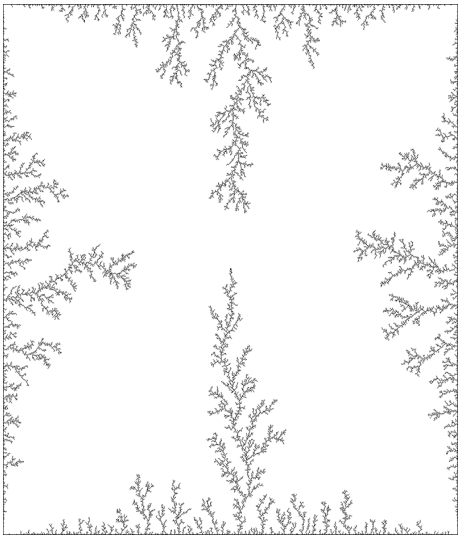

Figure 1.4: Box attractor, [5]

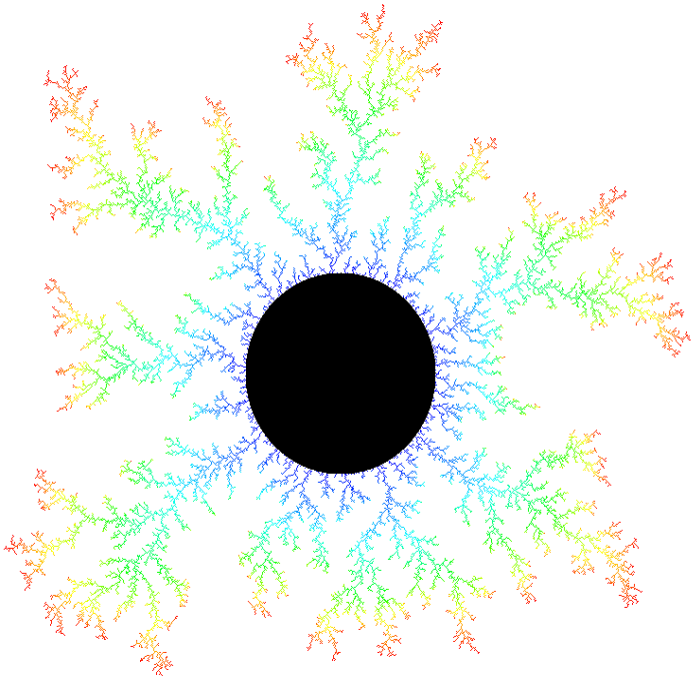

Figure 1.5: Circular attractor, [5]. The red particles have attached most recently to the cluster and are concentrated at the tips of the growing branches.

Chapter 2

Instability

An important ingredient in the study of patter formation is the stability of the moving interface. The competition between stabilising and destabilising effects on the evolving boundary is important for the pattern selection; Mullins and Sekerka worked with solidification fronts and considered both spherical and planar surfaces undergoing growth controlled by thermal or chemical diffusion fields. Even though these simple, theoretical models are now superseded, they still represent a general approach to gaining basic insight into several different types of pattern-forming processes.

2.1 Mullins-Sekerka instability on a circle

In this section our aim is to try to understand the instabilities issues using a simple example on a circle. Let us consider a circular surface that is growing in a Laplacian field U, which in this example represent concentration. The Laplacian growth process means that the normal velocity of the surface is proportional to the gradient of the local field, i.e.

$$v_n \sim |\nabla U|, \tag{2.1}$$

where U obeys the Laplace's equation in polar coordinates

$$\Delta U(r, \theta) \, = \, 0. \tag{2.2}$$

The circle has an original radius $\mathcal{R}_0$, and is deformed by a small perturbation $\varepsilon\cos(m\theta), m \geq 1$, such that the equation for the local radius $\mathcal{R}(\theta)$ of the circle reads

$$\mathcal{R}(\theta) \;=\; \mathcal{R}_0 \;+\; \varepsilon\, cos(m\,\theta), \tag{2.3}$$

where the amplitude of the pertubation is time dependent, i.e., $\varepsilon = \varepsilon(t)$, and initially small enough that the second and higher order terms in ε can be neglected.
If we assume that dilute theory holds, the equilibrium concentration $U_s(\theta)$ on the surface $\mathcal{R}(\theta)$ is determined by the capillarity condition

$$U_s(\theta) \;=\; U_0(1 + \gamma_C\kappa(\theta)). \tag{2.4}$$

Here U_0 is the concentration at equilibrium with a flat interface (for which $\kappa = 0$), $\gamma_C = \dfrac{\gamma V}{RT}$, where R is the gas constant, T is the temperature, V is the molar volume of the relevant material, γ is the surface tension and $\kappa(\theta)$ is the curvature of the surface. The curvature of an arc $s(\theta)$ that is parametrized in polar coordinates in given by

$$\kappa(\theta) \;=\; \frac{s^2(\theta) + 2(s'(\theta))^2 - s(\theta)s''(\theta)}{(s^2(\theta) + (s'(\theta))^2)^{\frac{3}{2}}},$$

which in the current example, remembering the neglected terms in ε, leads to

$$\kappa(\theta) \;=\; \frac{\mathcal{R}_0 + (m^2 - 1)\varepsilon\cos(m\theta)}{\mathcal{R}_0^2}. \tag{2.5}$$

The boundary condition at the surface $\mathcal{R}(\theta)$ then reads

$$U_s(\theta) \;=\; U_0\left(1 + \frac{\gamma_C}{\mathcal{R}_0^2}[\mathcal{R}_0 + (m^2 - 1)\varepsilon\cos(m\theta)]\right). \tag{2.6}$$

With r the distance from the center of the circle, the expression

$$U(r,\theta) \;=\; A\log r \;+\; \frac{B\varepsilon\cos(m\theta)}{r^m} \tag{2.7}$$

is a solution of the Laplace's equation, satisfying the boundary condition that the flux at infinity should be unaffected by the perturbation. The field around and unperturped circle behaves like $U(r) \sim \log|r|$, which is therefore also how $U(r,\theta)$ in (2.7) must behave as $r \to \infty$. Recalling the hypotesis on ε and remembering that, for ε small enough,

$$\log\left(1 + \frac{\varepsilon\cos(m\theta)}{\mathcal{R}_0}\right) \sim \frac{\varepsilon\cos(m\theta)}{\mathcal{R}_0},$$

at the surface $\mathcal{R}(\theta)$, Eq. (2.7) reads

$$U(\mathcal{R}(\theta)) \;=\; A\log\mathcal{R}_0 + \varepsilon\cos(m\theta)\left[\frac{A}{\mathcal{R}_0}+\frac{B}{\mathcal{R}_0^m}\right], \tag{2.8}$$

which must be equal to equation (2.6). A and B are determined by equating the coefficients of like harmonics in this boundary condition expression. The final result for the field U reads

$$U(r,\theta) \;=\; \frac{\log r}{\log\mathcal{R}_0}U_0\left(1+\frac{\gamma_C}{\mathcal{R}_0}\right)+\frac{\varepsilon\cos(m\theta)\mathcal{R}_0^{m-2}U_0}{r^m}\left(\gamma_C(m^2-1)-\frac{\gamma_C+\mathcal{R}_0}{\log\mathcal{R}_0}\right). \tag{2.9}$$

The normal velocity of the interface is proportional to the gradient of (2.9). For small perturbation it is sufficient to consider the radial derivative of $U(r,\theta)$, which leads to

$$v_n \;=\; \frac{d\mathcal{R}_0}{dt}+\frac{d\varepsilon}{dt}cos(m\theta) \;=\; \frac{\partial U(r,\theta)}{\partial r}\;|_{r=\mathcal{R}(\theta)}\;.$$

By again equating the coefficients of like harmonics , we have the following expressions:

$$\frac{d\mathcal{R}_0}{dt} \;=\; \frac{U_R}{\mathcal{R}_0\log\mathcal{R}_0} \tag{2.10}$$

$$\frac{1}{\varepsilon}\frac{d\varepsilon}{dt} \;=\; \frac{U_R(m-1)}{\mathcal{R}_0^2\log\mathcal{R}_0}-\frac{U_0\gamma_C}{\mathcal{R}_0^3}(m^3-m), \tag{2.11}$$

where $U_R \;=\; U_0\left(1+\dfrac{\gamma_C}{\mathcal{R}_0}\right)$ is the equilibrium concentration on an unperturbed circle, for which the curvature reads $\kappa \;=\; \dfrac{1}{\mathcal{R}_0}$.

Equation (2.11) is the growth rate of the perturbation amplitude and consists of two parts: the last term is the capillary effect and the other is the gradient term. The capillary effect is proportional to γ_C and the surface tension. It is negative and therefore it favours a decay of the perturbation. The gradient term is always positive and proportional to U_R and favours growth. In the absence of surface tension, the capillary effect vanishes and there is nothing to stabilise the surface. It is understood that the surface then takes on a uniform concentration, regardless of the shape. At the same time, it is known that the concentration at infinity is unaffected by any irregularities on the interface. This means that the change in concentration between the interface and infinity is everywhere the same, such that isoconcentration lines must be more densely packed above buldges than

at depressions. This gives a steeper concentration gradient and larger surface velocity at protuberances, which causes buldges to grow unstably. This is the action of the gradient term. Whenever surface tension is present, the capillary effect is opposing this instability. The curvature is positive for protuberances and negative for depressions, and it is larger in absolute value for small buldges than for large ones.
In general both effects will be present, and the stability of the surface will be determined by the competition between them.

2.1.1 Numerical visualization withouth surface tension

In this section we are going to analyze the previous phenomena from a numerical point of view. In particular we want to visualize the evolution of the boundary of a slightly perturbed circle under the Laplacian Growth process.
In our specific case, let's solve the Poisson Equation (A.1) in a circle with an hole; in particular such hole represent our perturbed circle; for this simulation we used, in (2.3), $\varepsilon = 0.01$ and different kind of values for m. Denoting with C the external cirle and Γ_t the internal distorted circle, we are going to solve the following problem:

$$\begin{cases} \Delta u(\cdot,t) \;=\; 0 & \text{in } C \setminus \Gamma_t \\ u(\cdot,t) \;=\; 1 & \text{on } \partial C,\ \forall\, t \in [0,T] \\ u(\cdot,t) \;=\; 0 & \text{on } \partial\Gamma_t,\ \ t \in [0,T] \\ \mathcal{V} \;=\; \vec{\nabla} u & \text{on } \ \Gamma_t,\ t \in [0,T] \end{cases} \tag{2.12}$$

where T is a fixed final time and $\mathcal{V}$ is the normal velocity of the interface $\partial\Gamma_t$. In order to solve this problem, we used the FreeFem++ software; a weak formulation of the Poisson equation is provided and the following step are performed:

- Solve the Poisson equation imposing homogeneous Dirichlet boundary condition on the internal perturbed circle, and $u = 1$ on the external one;
- Once the solution is provided, the gradient of the solution is computed in order to perform the Laplacian Growth;
- With the command `movemesh` the previous mesh is moved according to the direction of the gradient;

- With the command `adaptmesh` the mesh is well adapted to the new shape of the internal boundary;
- Go back to the first point and redo the computation for a fixed number of iterations (in our case $N = 100$).

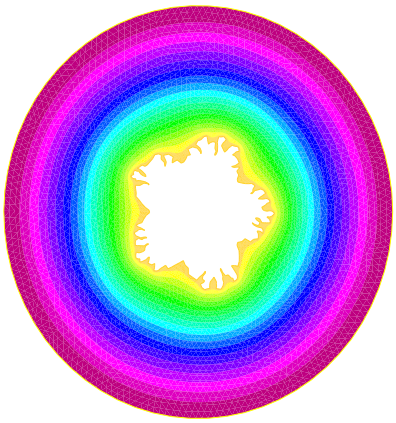

Figure 2.1: $m = 5$

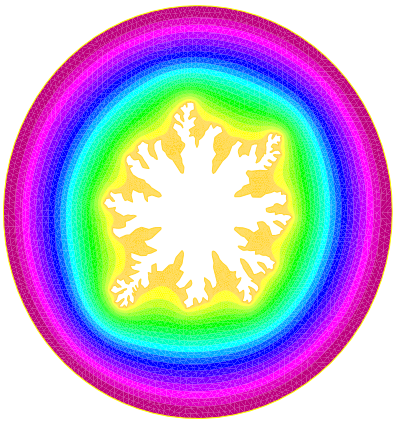

Figure 2.2: $m = 8$

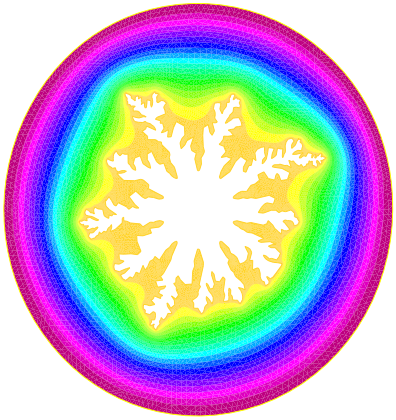

Figure 2.3: $m = 10$

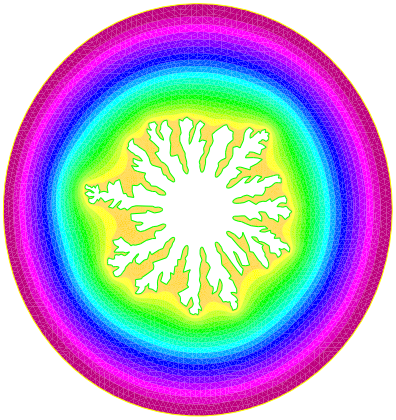

Figure 2.4: $m = 15$

All the complete code can be seen in Appendix C.1; With the previous setting, the solution can be seen in Figures [2.1 - 2.4]. As one can see, in this solution we have not

included the surface tension, hence according to formula (2.11), there is no the second term that curbs the instability.

Remark 2.1.1. As example, let us consider a three-fold perturbation of a circular bubble, whose exact dynamics without surface tension is shown in Fig. 1.1. If one tries to compute numerically the solution *withouth* including surface tension, the evolution is very similar until the cusps begin to form, at which point the tips bulge outward and split into new fingers; this process repeats itself to produce a complicated fractal pattern (Figure 2.10). In the next Figures [2.5 - 2.10] one can see this process evolving in time.

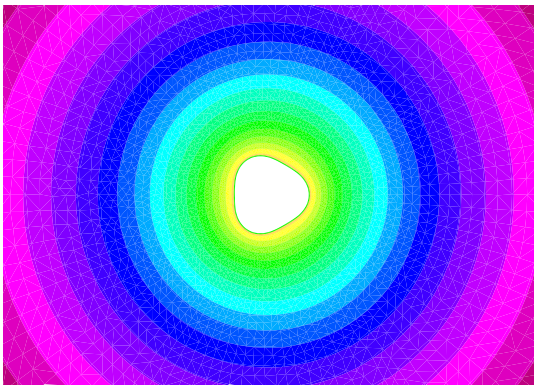

Figure 2.5: Niter = 1

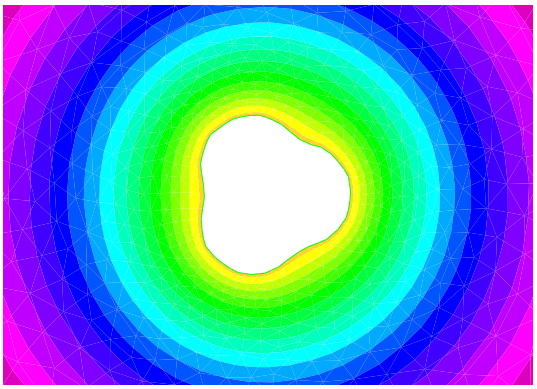

Figure 2.6: Niter = 500

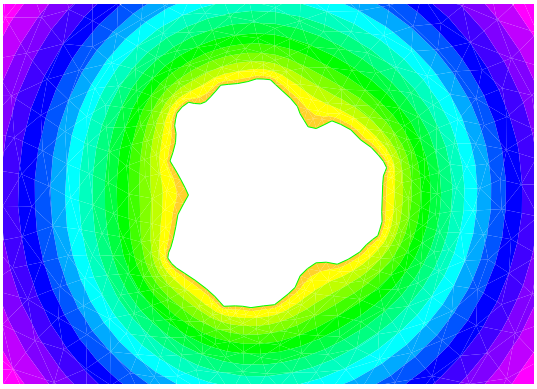

Figure 2.7: Niter = 1000

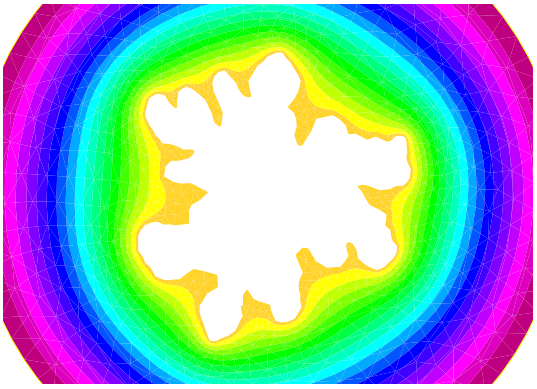

Figure 2.8: Niter = 2000

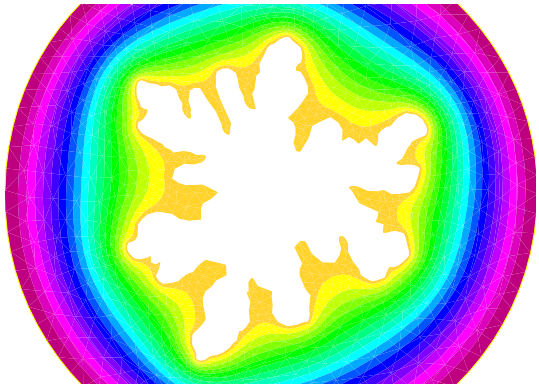

Figure 2.9: Niter = 2500

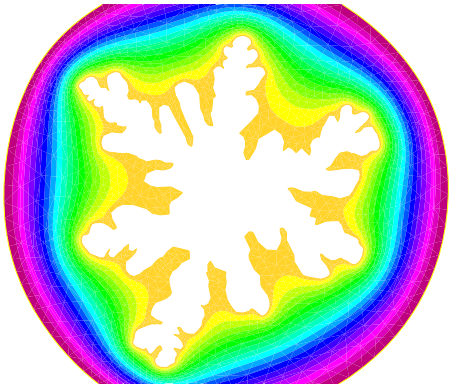

Figure 2.10: Niter = 3000

From this example one can understand that, *although* we have not included surface tension yet, the only numerical approximation works as an *artificial* surface tension, preventing the cups' formation.

2.1.2 Numerical visualization with surface tension

Let us now consider *surface tension* in our model; in particular, with the same notation of the previous section, we are going to solve the following problem:

$$\begin{cases} \Delta u(\cdot,t) = 0 & \text{in } C \setminus \Gamma_t \\ u(\cdot,t) = 1 & \text{on } \partial C,\ \forall\, t \in [0,T] \\ u(\cdot,t) = \gamma\, k(\cdot,t) & \text{on } \partial\Gamma_t,\ \ t \in [0,T] \\ \mathcal{V} = \vec{\nabla} u & \text{on } \Gamma_t,\ t \in [0,T] \end{cases} \tag{2.13}$$

where $k(\cdot,t)$ denotes the curvature of the internal perturbed circle at each time step and γ is a constant, called the *surface tension*, which is relevant is order to give a weight to the curvature's influence: if it is too small, surface tension's effect will not occurs, while if too big, any growth will start; for a specific constant γ it will be possible to study the real effect of the surface tension in the model. Starting from the same shape of example 2.1.1, we vary the mesh size in a decreasing way and plot the results including or not surface tension boundary condition (Figure 2.11). Denoting h the mesh size, in these three simulations we have used $h = [0.6, 0.4, 0.2]$. One can immediately realize that

including surface tension lead to convergence of the solution, while if one performs zero boundary conditions, hence the surface tension is not included in the model, the result is very effected by the number of triangles.

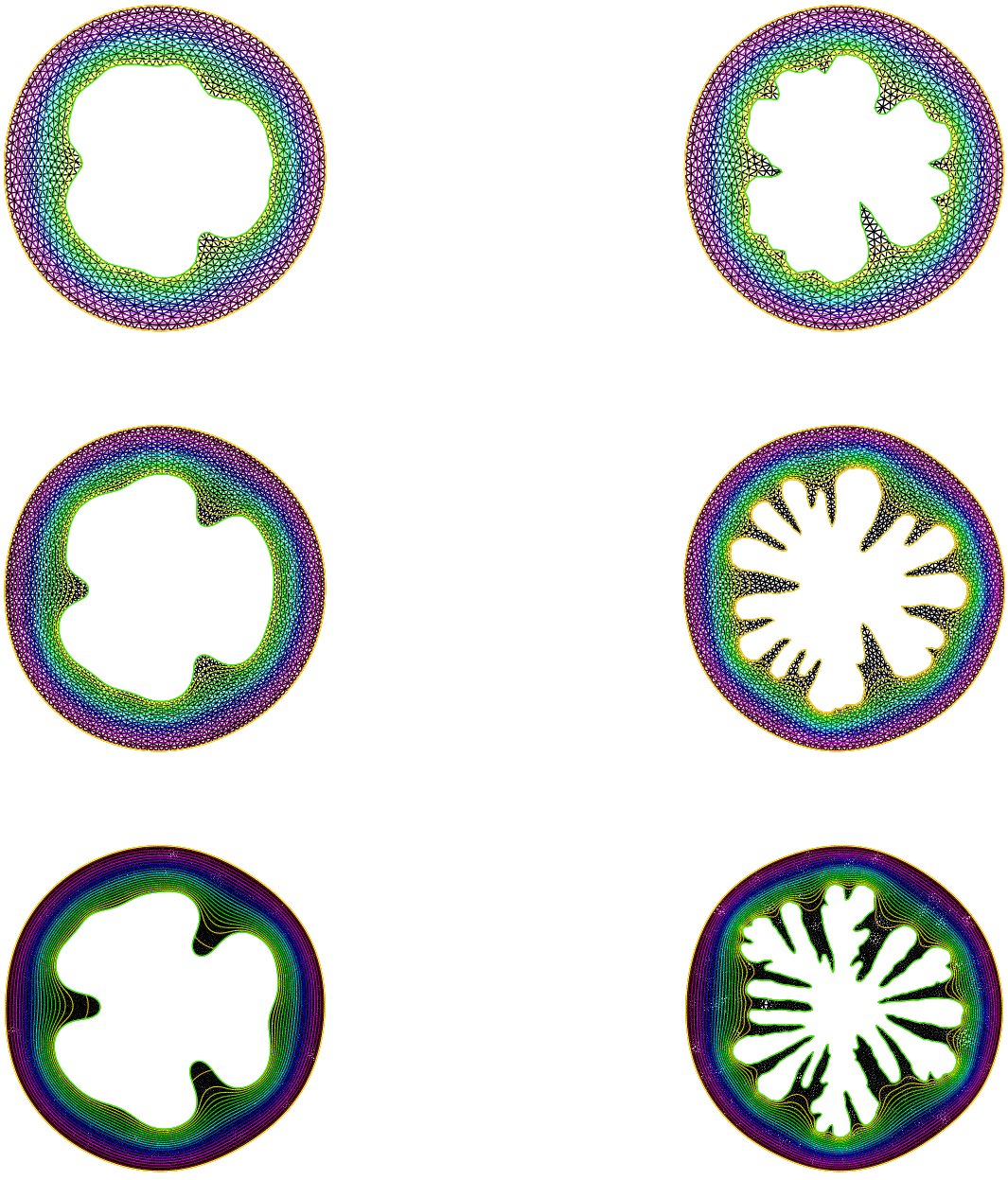

Figure 2.11: From the top to the bottom: at the left hand side surface tension is included while at the right hand side zero boundary condtions are implemented. ($m = 3$)

The same simulation has been done starting from a five-fold perturbation, i.e. $m = 5$. (Figure 2.12). Here, the convergence at the left hand side is even more clear.

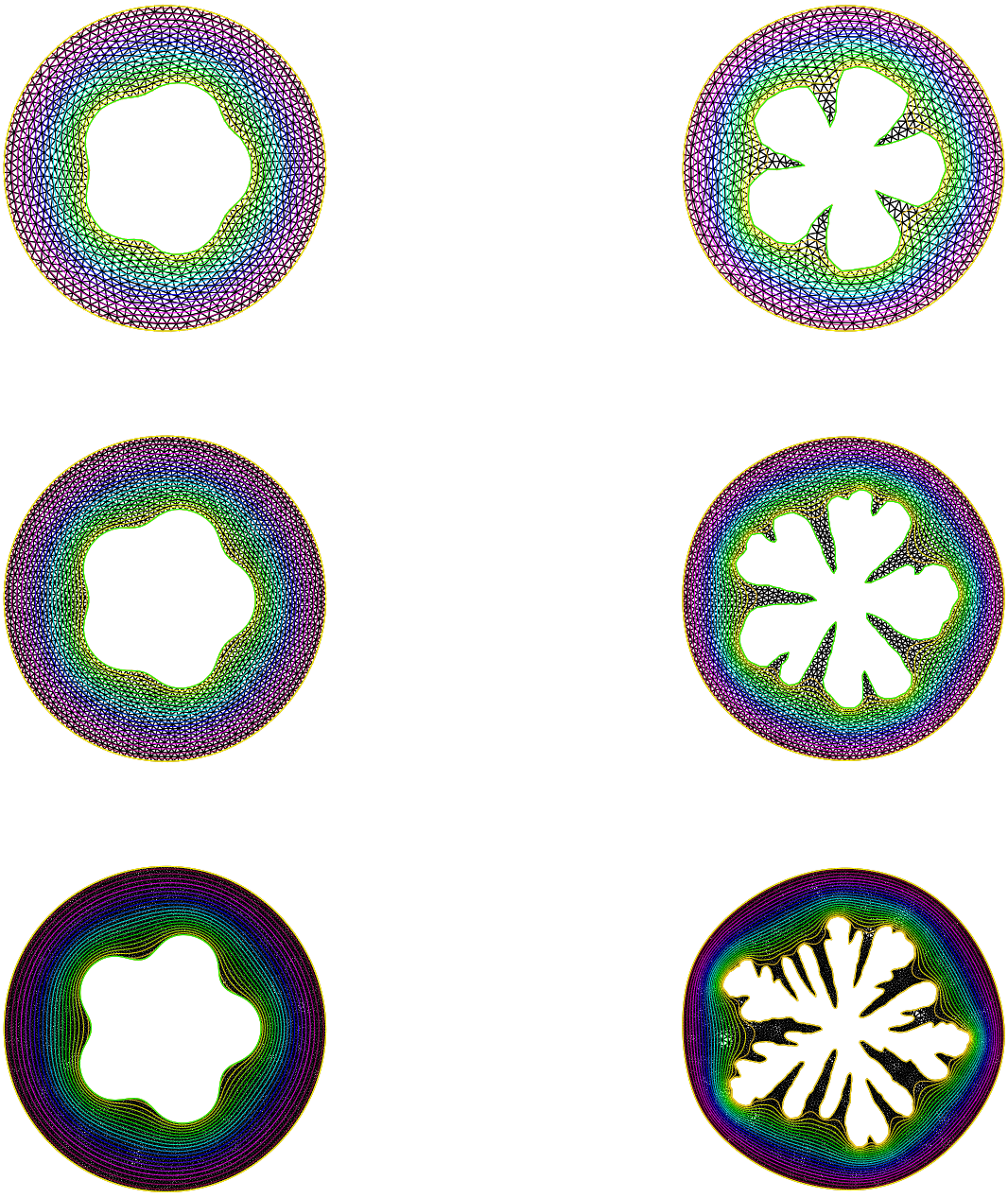

Figure 2.12: From the top to the bottom: at the left hand side surface tension is included while at the right hand side zero boundary condtions are implemented. ($m = 5$)

Concluding, *surface tension* acts as a regularizer of the solution, providing a result which does not depend on the mesh size.

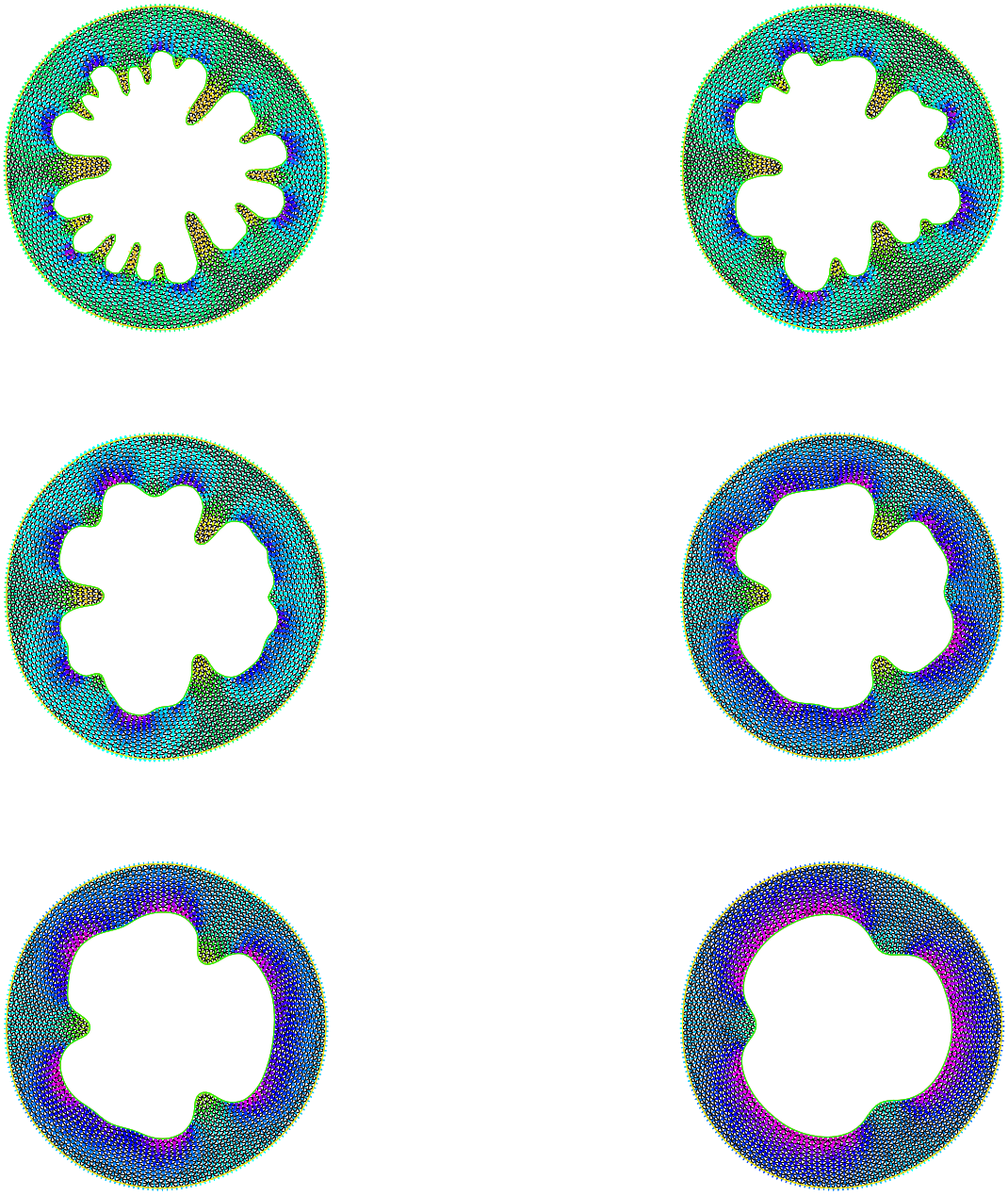

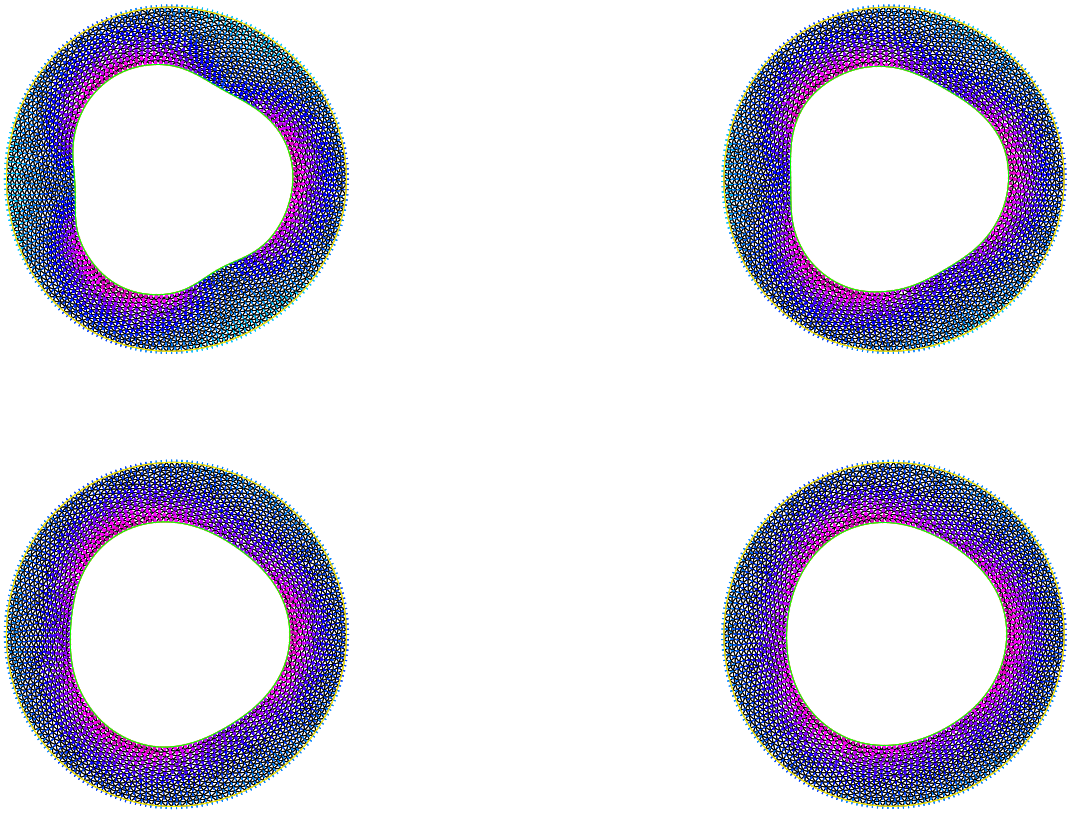

Figure 2.13: From the left to the right: Surface Tension effect as regularizer of the solution

In Figure 2.13 one can see the real effect of the surface tension as a regularizer of the solution. In these ten plots the number of triangles is fixed, while the coefficient γ in (2.13) increases, i.e. the effect of surface tension on the final solution growth. In particular $\gamma = [0.004, 0.008, 0.012, 0.016, 0.02, 0.03, 0.05, 0.07, 0.09, 0, 1]$. As one can see in the last 3 plots the effect of the surface tension prevents completely the instabilities' growth and, moreover, in the final plot also the initial instabilities of the interface are deleted, returning a quite circular shape, completely according to Equation (2.11). The complete code can be found again in Appendix C.1.

2.2 Mullins-Sekerka instability on a sphere

2.2.1 Spherical Harmonics

Spherical harmonics are a set of functions used to represent functions on the surface of the sphere $\mathbb{S}^2$. They are a higher dimensional analogy of Fourier series, which form a complete basis for the set of periodic functions of a single variable. Spherical armonics are defined as the eigenfunctions of the angular part of the Laplacian in three dimensions. As a result, they are extremely convenient in representing solutions to PDEs in which the Laplacian appears, e.g. the Poisson equation. The construction of these harmonics is analogous to the case of the usual trigonometric functions $\sin(m\phi)$ and $\cos(m\phi)$ which form a complete basis for the periodic functions of a single variable (the Fourier Series) and are eigenfunctions of the angular Laplacian in two dimensions $\Delta_\phi = \dfrac{\partial^2}{\partial\phi^2}$, with eigenvalue $-m^2$. The three-dimensional Laplacian in spherical coordinates

$$\begin{cases} x = r\sin\theta\cos\phi \\ y = r\sin\theta\sin\phi \\ z = r\cos\theta \end{cases} \tag{2.14}$$

takes the form

$$\Delta = \frac{1}{r^2\sin\theta}\left(\frac{\partial}{\partial r}r^2\sin\theta\frac{\partial}{\partial r} + \frac{\partial}{\partial\theta}\sin\theta\frac{\partial}{\partial\theta} + \frac{\partial}{\partial\phi}\csc\theta\frac{\partial}{\partial\phi}\right). \tag{2.15}$$

The Laplace equation $\Delta u = 0$ can be solved via separation of variables. We make the ansatz $u(r,\theta,\phi) = R(r)Y(\theta,\phi)$ to separate the radial and angular parts of the solution. In spherical coordinates, one obtains the two eigenvalue equations for $R(r)$ and $Y(\theta,\phi)$:

$$\frac{\partial}{\partial r}\left(r^2\frac{\partial R(r)}{\partial r}\right) = l(l+1)R(r) \tag{2.16}$$

$$\frac{1}{\sin\theta}\frac{\partial}{\partial\theta}\left(\sin\theta\frac{\partial Y(\theta,\phi)}{\partial\theta}\right) + \frac{1}{\sin^2\theta}\frac{\partial^2 Y(\theta,\phi)}{\partial\phi^2} = -l(l+1)Y(\theta,\phi), \tag{2.17}$$

where $l(l+1)$ is some constant called the *separation constant*, written in the most convenient form. The angular part can also be solved by separation of variables. We

make the ansatz $Y(\theta,\phi) = \Theta(\theta)e^{im\phi}$ for some second separation constant m which can take negative values. This gives the equation for $\Theta(\theta)$:

$$\sin\theta\frac{\partial}{\partial\theta}\left(\sin\theta\frac{\partial\Theta(\theta)}{\partial\theta}\right) = m^2\Theta(\theta) - l(l+1)\sin^2\theta\,\Theta(\theta).$$

The solutions for $\Theta(\theta)$ can be found by putting the equation into a canonical form, the solutions of which are given in terms of the Legendre Polynomials:

$$P_l^m(x) = \frac{(-1)^m}{2^l l!}(1-x^2)^{m/2}\frac{d^{l+m}}{dx^{l+m}}(x^2-1)^l.$$

The general solution for each linearly independent $Y(\theta,\phi)$ are the spherical harmonics, with a normalization constants multiplying the solution to make independent spherical harmonics orthonormal:

$$Y_l^m(\theta,\phi) = \sqrt{\frac{2l+1}{4\pi}\frac{(l-m)!}{(l+m)!}}\,P_l^m(\cos\theta)e^{im\phi}. \tag{2.18}$$

Every spherical harmonic is labeled by the integers l and m, the *order* and *degree* of a solution. Some of the low-lying spherical harmonics are enumerated in the table below, as derived from the above formula:

l	m	$Y_l^m(\theta,\phi)$
0	0	$\sqrt{\frac{1}{4\pi}}$
1	-1	$\sqrt{\frac{3}{8\pi}}\sin\theta e^{-i\phi}$
1	0	$\sqrt{\frac{3}{4\pi}}\cos\theta$
1	1	$-\sqrt{\frac{3}{8\pi}}\sin\theta e^{i\phi}$
2	-2	$\sqrt{\frac{15}{32\pi}}\sin^2\theta e^{-2i\phi}$
2	-1	$\sqrt{\frac{15}{8\pi}}\sin\theta\cos\theta e^{-i\phi}$
2	0	$\sqrt{\frac{5}{16\pi}}(3\cos^2\theta-1)$
2	1	$-\sqrt{\frac{15}{8\pi}}\sin\theta\cos\theta e^{i\phi}$
2	2	$-\sqrt{\frac{15}{32\pi}}\sin^2\theta e^{2i\phi}$

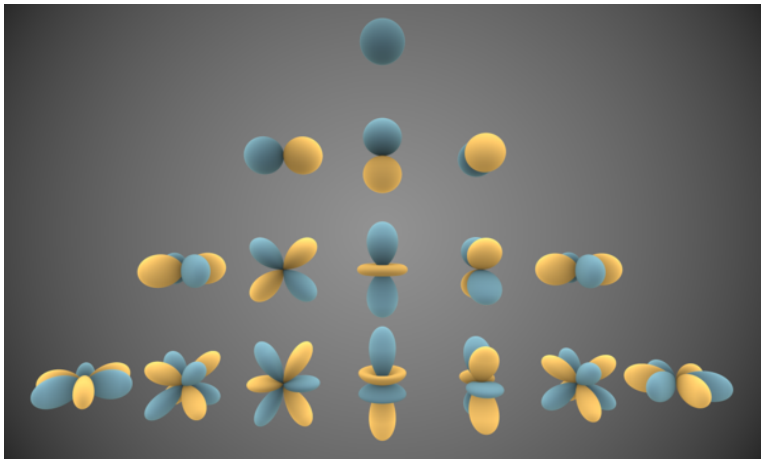

Figure 2.14: Visual representations of the first few real spherical harmonics. Blue portions represent regions where the function is positive, and yellow portions represent where it is negative. The distance of the surface from the origin indicates the absolute value of $Y_l^m(\theta, \phi)$ in the angular direction (θ, ϕ).

2.2.2 Stability analysis

In this section we want to summarize the fundamental paper of Mullins-Sekerka [1]. The stability of the shape of a spherical particle undergoing diffusion-controlled growth is studied by supposing an expansion, into spherical harmonics, of an infinitesimal deviation of the particle from sphericity and then calculating the time dependence of the coefficients of the expansion. It is assumed that the concentration field obeys Laplace's equation. Let's start observing that the diffusion-controlled is characterized by the velocity v with which each element of its interface moves according to the equation

$$v = \left[\frac{D}{C - c_s}\right] \frac{\partial c}{\partial n}, \tag{2.19}$$

where D is the diffusion coefficient, c is the position dependent concentration, $\partial c/\partial n$ is the normal derivative of the concentration at the interface and c_s denote the equilibrium value of c at a general interface (possibly curved). We first investigate the behaviour of an infinitesimal distorsion of a sphere caused by a single spherical harmonic Y_l^m; the behaviour of an arbitrary infinitesimal distorsion may then be obtained by superposition

since all equations are linear. The equation of the distorted sphere reads:

$$\rho(\theta,\phi) \;=\; R \;+\; \delta Y_l^m(\theta,\phi), \tag{2.20}$$

where R is the initial sphere and δ is very small, so that powers higher than the first may be neglected. Notice that $\rho, \mathcal{R}_0$ and δ depend on the time. As in the 2D case, if we assume that dilute solution holds, the equilibrium cincentration $c_s(\theta,\phi)$ on the surface $\rho(\theta,\phi)$ is determined by the capillarity condition

$$c_s \;=\; c_0(1+\Gamma_D K), \tag{2.21}$$

where c_0 denotes the equilibrium value of c at a flat interface, K is the mean curvature and $\Gamma_D \;=\; (\gamma\Omega)/(RT)$ is a capillarity constant in which γ is the interfacial free energy, Ω the increment of volume per mole of added solute, R is the gas constant, and T the absolute temperature; tipically $\Gamma_D \approx 10^{-7}$ cm. By utilizing the fact that the curvature K of a surface $z(x,y)$ which deviates only slightly from flatness may be calculated from the expression $K = -\nabla^2 z$, it is easily shown that the curvature $K(\theta,\phi)$ at all points of the slightly distorted sphere $r(\theta,\phi) \;=\; R + \delta g(\theta,\phi)$ is given by the expression:

$$K(\theta,\phi) \;=\; \frac{2}{R}\left(1-\frac{\delta g}{R}\right) - \frac{\delta\Lambda g}{R^2} \tag{2.22}$$

where Λ is the angular part of the Laplacian operator expressed in spherical coordinates, namely

$$\Lambda \;=\; \frac{1}{\sin\theta}\frac{\partial}{\partial\theta}\left(\sin\theta\frac{\partial}{\partial\theta}\right) + \frac{1}{\sin^2\theta}\frac{\partial^2}{\partial\phi^2}.$$

Substituting Y_l^m for g in (2.22), utilizing (2.16) (i.e. $\Lambda Y_l^m \;=\; -l(l+1)Y_l^m$) and then substituting the resulting expression for K into (2.21), we obtain the expression of the equilibrium concentration $c_s(\theta,\phi)$ on the distorted sphere

$$c_s(\theta,\phi) \;=\; c_0\left[1+\frac{2\Gamma_D}{R}+\frac{\Gamma_D\delta Y_l^m}{R^2}(l+2)(l-1)\right]. \tag{2.23}$$

We look for a solution of Laplace's equation which reduces to Eq. (2.23) on the surface given by Eq. (2.20). We can consider the expression

$$c(r,\theta,\phi) \;=\; \frac{A}{r}+\frac{B\delta Y_l^m}{r^{l+1}}+c_\infty, \tag{2.24}$$

which satisfies Laplace's equation and which reduces to the value c_∞ at $r = \infty$. Recalling that for $x \to 0$, $\frac{1}{1+x} \simeq 1 - x$, the value of this expression on the surface $\rho(\theta, \phi)$ (Eq. (2.20)) to first order in δ is

$$c(\rho, \theta, \phi) \;=\; \frac{A}{R}\left(1 - \frac{\delta Y_l^m}{R}\right) + \frac{B\delta Y_l^m}{R^{l+1}} + c_\infty.$$

Since this expression must be equal to Eq. (2.23), and since the expansion in harmonics is unique, A and B are easily determined by equating coefficients of like harmonics. Indeed we have the following system

$$\begin{cases} \dfrac{A}{R} + c_\infty \;=\; c_0 + \dfrac{2\Gamma_D c_0}{R} \\[2ex] \dfrac{B}{R^{l+1}} - \dfrac{A}{R^2} \;=\; \dfrac{c_0 \Gamma_D}{R^2}(l+2)(l-1). \end{cases} \tag{2.25}$$

Thus the resulting solution $c(r, \theta, \phi)$ of Laplace's equation which obeys all boundary conditions is:

$$c(r, \theta, \phi) \;=\; \frac{R(c_0 - c_\infty) + 2\Gamma_D c_0}{r} + \frac{\{(c_0 - c_\infty)R^l + c_0 \Gamma_D R^{l-1} l(l+1)\}\delta Y_l^m}{r^{l+1}} + c_\infty. \tag{2.26}$$

In order to complete the analysis we have to compute the velocity of the interface. Since the deviation of the tangent plane of the particle from that of the original sphere is infinitesimal at all points, it sufficies to take the radial derivative to find the velocity:

$$v \;=\; \frac{dR}{dt} \;+\; \frac{d\delta}{dt} Y_l^m \tag{2.27}$$

Moreover we know that the velocity at the interface is given by Eq. (2.19), i.e.

$$v \;=\; \frac{D}{C - c_s}\left(\frac{\partial c}{\partial r}\right)_{r=\rho} \;= \tag{2.28}$$

$$= \frac{D}{C - c_s}\left\{\frac{c_\infty - c_R}{R} + \left[(l-1)\frac{c_\infty - c_0}{R^2} - \frac{c_0 \Gamma_D}{R^3}[l(l+1)^2 - 4]\right]\delta Y_l^m\right\}, \tag{2.29}$$

where $c_R = c_0[1 + (2\Gamma_D/R)]$ is the concentration on the undistorted sphere. Equating coefficients of the harmonics, we obtain the rate of growth $d\delta/dt$ of the amplitude of the

spherical harmonic:

$$\frac{1}{\delta_l}\frac{d\delta_l}{dt} = \frac{c_0 D(l-1)}{(C-c_R)R^2}\left[\frac{c_\infty - c_0}{c_0} - \frac{\Gamma_D}{R}[(l+1)(l+2)+2]\right] \tag{2.30}$$

$$= \frac{D(l-1)}{(C-c_R)R}\left[G - \frac{c_0\Gamma_D}{R^2}(l+1)(l+2)\right], \tag{2.31}$$

where $G = (c_\infty - c_R)/R$ is the normal concentration gradient at the surface of the undistorted sphere; the amplitude has been labeled with the subscript l to indicate the harmonic to which it corresponds.

Equation (2.30) shows that the evolution of the perturbation is composed by two terms: a positive term proportional to G, which represents a gradient effect favoring the growth of the harmonic, and a negative term proportional to Γ_D, which represent a capillary effect favoring decay of the harmonic. The pure gradient effect is realized when γ (and hence Γ_D) vanishes so that the surface assumes a uniform concentration. The pure capillary effect is realized when G vanishes. In general, both gradient and capillary effect are present and the question of stability reduces to the study of which effect dominates. Evidently, all harmonics for which the bracket of Eq. (2.30) is positive must grow; they correspond to values of l which satisy the inequality

$$(l+1)(l+2)+2 < \frac{R(c_\infty - c_0)}{\Gamma_D c_0}. \tag{2.32}$$

All higher armonics for which the inequality is reversed must decay. Again it follows from Eq. (2.30) that a harmonic of a given l will grow or will decay according, respictively, to whether the radius of the sphere is greater than or is less than the critical value

$$R_c(l) = \left[\frac{1}{2}(l+1)(l+2)+1\right]R^*, \tag{2.33}$$

where $R^* = \dfrac{2\Gamma_D c_0}{c_\infty - c_0}$. The quantity R^* is the critical radius (corresponding to $c_R = c_\infty$) above which the sphere itself grows and below which it shrinks.

Chapter 3

Coral's growth simulation

In this Chapter we are going to simulate the Coral's growth in dimension 2. In particular we will start with the basic simulation of a Laplacian growth, i.e. where the growth is only affected by the concentration gradient of the solution of the Laplace's equation. After this simulation, we will introduce the advection diffusion equation and the Stokes equation, in order to simulate a coral's growth where the concentration of nutrients is affected by the flow given by the solution of the Stokes equation.

3.1 Laplacian growth in 2D

In this section a first basic model of coral's growth will be introduced. In particular the domain of the simulation will be the rectangle $\Omega_t = R \setminus \Gamma_t$ where $R = ([0, L_x] \times [0, L_y])$ and Γ_t represent the simulated coral, with Γ_0 given by the circle

$$\Gamma_0 := \{(x, y) : (x - L_x/2)^2 + (y - L_y/10)^2 \leq (L_y/10)^2\}$$

So basically, at time $t = 0$, the simulated coral is given by a circle resting on the ground. The initial domain with the initial mesh can be seen in Figure 3.1. The idea is to perform an evolution of $\Lambda(t) := \partial\Gamma_t$ in order to let the coral growth. Let us start with denoting

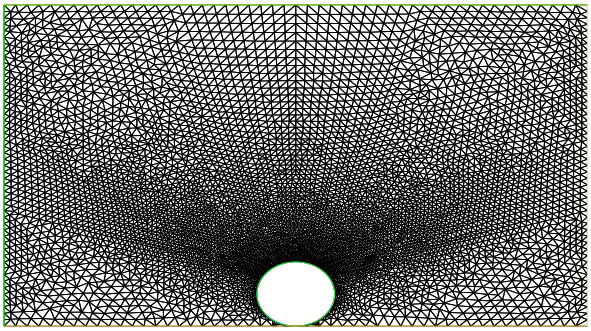

Figure 3.1: Initial mesh

$\partial\Omega_t = \Gamma_{\text{in}} \cup \Gamma_{\text{out}} \cup \Gamma_{\text{bott}} \cup \Gamma_{\text{top}} \cup \Lambda_t$ the boundary of the domain Ω_t where

$$\begin{aligned} \Gamma_{bott} &= [0, L_x] \times \{0\} \\ \Gamma_{\text{in}} &= \{0\} \times [0, L_y] \\ \Gamma_{\text{out}} &= \{L_x\} \times [0, L_y] \\ \Gamma_{\text{top}} &= [0, L_x] \times \{L_y\} \end{aligned}$$

First we have to solve the Laplace equation at each time step and then compute the evolution of the interface Λ_t according to the Laplacian growth theory. For small $T > 0$, we consider the following *free boundary problem*: finding a function $C(x,t)$, $(x,t) \in \Omega_t \times [0,T]$ and a free boundary $\Lambda = \cup_{t\in[0,T]}(\Lambda_t \times \{t\})$ satisfying

$$\begin{cases} -\Delta C(\cdot,t) = 0 & \text{in } \Omega_t, \ \ t \in [0,T] \\ C = C_0 & \text{on } \Gamma_{\text{top}} \times [0,T] \\ C = C_0 \left(\text{or } \dfrac{\partial C}{\partial n} = 0\right) & \text{on } (\Gamma_{\text{in}} \cup \Gamma_{\text{out}}) \times [0,T] \\ C = 0 & \text{on } \Lambda_t \cup \Gamma_{\text{bott}}, \ \ t \in [0,T] \\ \mathcal{V} = \vec{\nabla} C & \text{on } \Lambda_t, \ t \in [0,T] \\ \Omega_0 = ([0,L_x] \times [0,L_y]) \setminus \Gamma_0 & \text{on } \{t = 0\} \end{cases} \tag{3.1}$$

where $\mathcal{V}$ is the normal velocity of Λ_t. As one can see, two kind of boundary conditions have been implemeneted in order to simulate the coral growth. In both simulation we have supposed that che concentration of nutrients is set to be zero on the coral and on the ground.

In order to solve numerically the evolution (3.1), the same idea of Section 2.1.1 has been implemented, using the FreeFem command `movemesh` and `adaptmesh` in order to move the boundary. For this particular simulation we have used the following parameters: $L_x = 3$, $L_y = 2$, $C_0 = 10$. The result can be seen in Figures 3.2 - 3.3.

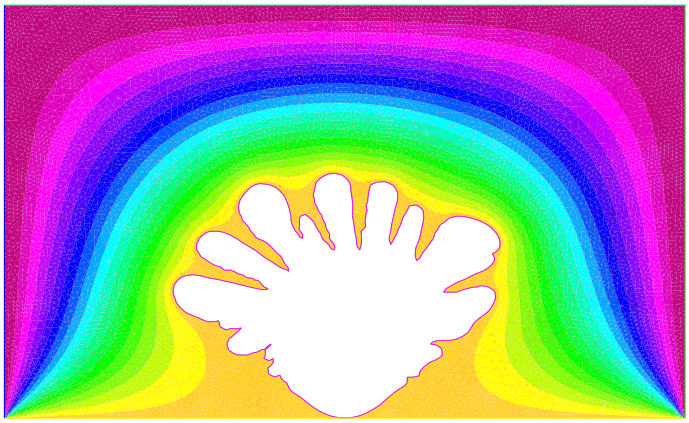

Figure 3.2: Simulation growth with Dirichlet BCs

Remark 3.1.1. As we mentioned, in the implementation of this kind of equations the command `movemesh` in essential in order to perform the movement of the interface. However, once the gradient of the solution is computed, of course it will not be zero on all the boundary and so some trick is needed in order to fix the boundary out of the coral and do not move it during the process. The idea is the following: Let's fix a time step where the solution C of the Poisson equation is computed, and so its gradient $\vec{\nabla}C$. In order to compute the vector field responsible for the movement of the interface, we

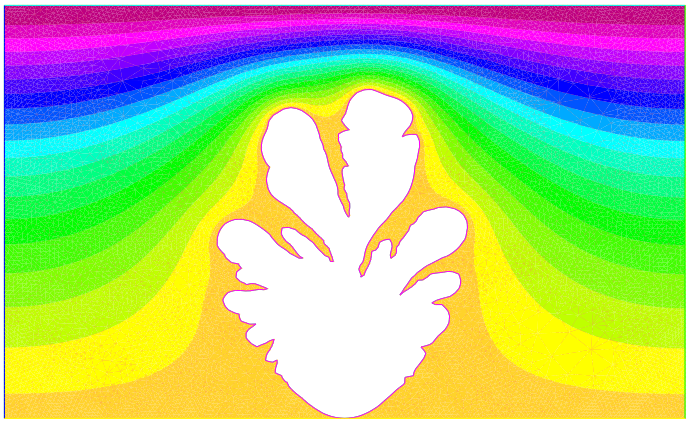

Figure 3.3: Simulation growth with Neumann BCs

will solve the following PDE:

$$\begin{cases} -\Delta\vec{U} = 0 & \text{in } \Omega_t \\ \vec{U} = 0 & \text{on } \partial R \\ \vec{U} = \vec{\nabla} C & \text{on } \Lambda_t \end{cases} \tag{3.2}$$

As one can see, the new vector field $\vec{U}$ will be zero on the rectangle and exactly the concentration gradient on the coral. In this way, using $\vec{U}$ as vector field for the movement of the mesh, we will ensure to move only the coral, as we want.

3.2 Fluid flow effect

In this section we are going to study the behaviour of the coral's growth under a more complex structure. In particular we will start solving the Stokes Equation in order to have a velocity field representing our fluid flow; then the stationary advection-diffusion equation will be solved in order to let the coral growth according to the gredient of

the solution, in the same way of the previous section. Let's briefly recall the equations involved in the process. In the case of a flow at low Reynolds number (for instance micro-organism) the Stokes equation holds, i.e.

$$\begin{cases} -\mu\Delta\mathbf{u} + \nabla p = 0 \\ \nabla \cdot \mathbf{u} = 0 \end{cases} \tag{3.3}$$

where $\mathbf{u} = (u_1, u_2)$ is the fluid velocity and p is the pressure. More details about this equation and the weak formulation of it used in order to implement it can be found in Appendix A.
The stationary advection-diffusion equation describes the steady-state behaviour of an advective-diffusive system; the PDE reads

$$-D\,\Delta C + \mathbf{u} \cdot \nabla C = 0 \tag{3.4}$$

where C indicates the concentration nutriments, D is the diffusivity (also called diffusion coefficient), $\mathbf{u}$ is the velocity field that the concentration is moving with (in our case will be the solution of the Stokes Equation).
In our study it will be very important the competition between the advective and the diffusive term. Indeed, fixing the solution of the Stokes Equation, i.e. the velocity, when the diffusion constant is small we will see that the advective part dominates, hence an asimmetric solution will occur. On the other side, when the diffusion coefficient growth, the coral's simmetry will be recovered, and a similar result of the previous section will appear.

Boundary conditions have to be imposed to the previous equations. The common boundary condition to all our following simulations is the *no slip* condition on $\Gamma_{\text{bott}} \cup \Lambda_t$, i.e.

$$\mathbf{u} = \mathbf{0} \quad \text{on } \Gamma_{\text{bott}} \cup \Lambda_t. \tag{3.5}$$

Moreover we will ask a Dirichlet Boundary condition on Γ_{in}, e.g. $\mathbf{u} = (1, 0)$, and Neumann Boundary conditions on the remaing boundary. With the same notation of the previous section, we will solve the following system in order to perform the moving of the interphase, i.e. the coral's growth:

$$
\begin{cases}
-\mu\Delta\mathbf{u}(\cdot,t) + \nabla p(\cdot,t) = 0 & \text{in } \Omega_t, \ \ t \in [0,T] \\
\nabla \cdot \mathbf{u}(\cdot,t) = 0 & t \in [0,T] \\
\mathbf{u} = \mathbf{0} & \text{on } \Gamma_{\text{bott}} \cup \Lambda_t \\
\mathbf{u} = (1,0) & \text{on } \Gamma_{\text{in}} \\
\mathbf{u}\cdot\mathbf{n} = 0 & \text{on } \Gamma_{\text{top}} \cup \Gamma_{\text{out}} \\
-D\,\Delta C(\cdot,t) + \mathbf{u}(\cdot,t)\cdot\nabla C(\cdot,t) = 0 & \text{in } \Omega_t, \ \ t \in [0,T] \\
C = C_0 & \text{on } \Gamma_{\text{top}} \times [0,T] \\
C = C_0 \left(\text{or } \dfrac{\partial C}{\partial n} = 0\right) & \text{on } (\Gamma_{\text{in}} \cup \Gamma_{\text{out}}) \times [0,T] \\
C = 0 & \text{on } \Lambda_t \cup \Gamma_{\text{bott}}, \ \ t \in [0,T] \\
\mathcal{V} = \vec{\nabla} C & \text{on } \Lambda_t, \ t \in [0,T] \\
\Omega_0 = ([0,L_x]\times[0,L_y]) \setminus \Gamma_0 & \text{on } \{t=0\}
\end{cases}
\tag{3.6}
$$

We can see the result of two simulations, Figure 3.4 where $D = 1$ and Figure 3.5 where $D = 0.01$. In both cases we setted $\mu = 1$. As one can see, in the second one, the advective part is relevant, providing an asymmetric behaviour of the coral.

Remark 3.2.1. Notice that one can implement different boundary conditions for the Advection-Diffusion equation. Indeed, since the nutriments are transported through the fluid flow, it is not the most natural choise to impose Dirichlet Boundary conditions on $\Gamma_{\text{top}} \cup \Gamma_{\text{out}}$; for instance we can impose Dirichlet Boundary condition just at the inlet and Neumann BCs on the rest of the boundary (apart from the usual homogeneous BCs on the coral and on the ground). Summarizying, after the Stokes Equation, the Advection-Diffusion equation reads

$$
\begin{cases}
-D\,\Delta C(\cdot,t) + \mathbf{u}(\cdot,t)\cdot\nabla C(\cdot,t) = 0 & \text{in } \Omega_t, \ \ t \in [0,T] \\
C = C_0 & \text{on } \Gamma_{\text{in}} \times [0,T] \\
\dfrac{\partial C}{\partial n} = 0 & \text{on } (\Gamma_{\text{top}} \cup \Gamma_{\text{out}}) \times [0,T] \\
C = 0 & \text{on } \Lambda_t \cup \Gamma_{\text{bott}}, \ \ t \in [0,T]
\end{cases}
$$

One simulation with these boundary conditions can be seen in Figure 3.6. Notice that also in this case, assimetric's growth appear; thus it can be caused by a predominant

advective part (i.e. law diffusion coefficient) or by different boundary conditions in the Advection-Diffusion equation.

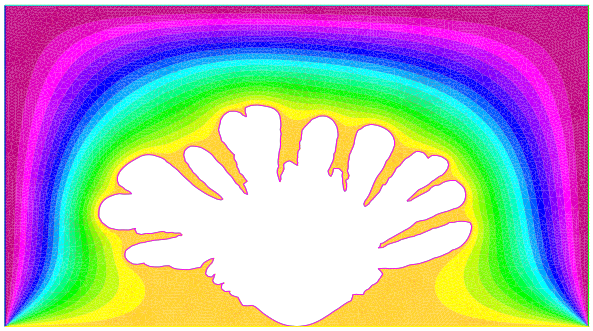

Figure 3.4: Simulation growth under fluid flow, $D = 1$

Figure 3.5: Simulation growth under fluid flow, $D = 0.01$

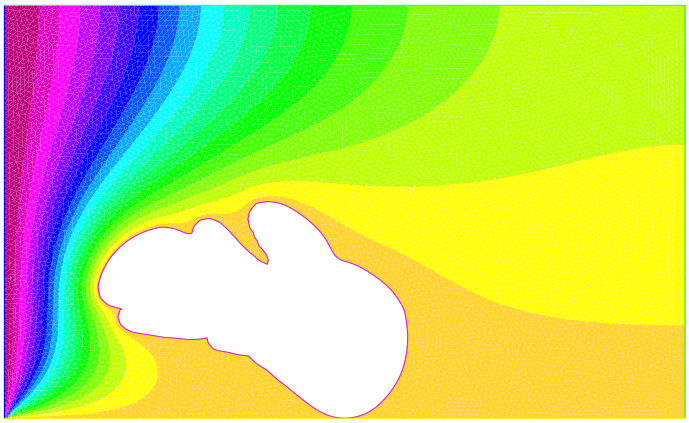

Figure 3.6: Simulation growth under fluid flow with Neumann BCS

Chapter 4

Future perspectives

The aim of this section is summarize the main points of the thesis and introduce future prespectives concerning few arguments that need to be further investigated.
Let's start with one of the problem that is more related with our PDE system for coral's growth, i.e. Equation (3.1). There is a huge variety of bibliography concerning free boundary problems; in particular, X. Chen (*et al.*) have studied the existence, uniqueness and regularity of classical and weak solution of the following Mullins-Sekerka problem: Let Ω be a bounded domain in $\mathbb{R}^n$ $(n \geq 2)$ and Γ_0 be the boundary of an open set $\Omega_0 \subset\subset \Omega$. For small $T > 0$, we consider the following free boundary problem: finding a function $u(x,t)$, $(x,t) \in \Omega \times (0,T)$ and a free boundary $\Gamma = \cup_{t\in[0,T]}(\Gamma_t \times \{t\})$ satisfying

$$\begin{cases} \Delta u(\cdot,t) = 0 & \text{in } \Omega \setminus \Gamma_t, \ \ t \in [0,T] \\ \partial_n u = 0 & \text{on } \partial\Omega \times [0,T] \\ u = -\mathcal{K} & \text{on } \Gamma_t,\ t \in [0,T] \\ \mathcal{V} = [\partial_n u] & \text{on } \Gamma_t,\ t \in [0,T] \\ \Gamma \cap \{t=0\} = \Gamma_0 & \text{on } \{t=0\} \end{cases} \tag{4.1}$$

where $\partial_n u$ is the outward normal derivative to $\partial\Omega$ and $[\partial_n u] = \partial_n^+ u + \partial_n^- u$ is the sum of the *outward* normal derivatives of u from each side of Γ_t (which is also equal to the jump of the normal derivatives of u facross Γ_t). Here $\mathcal{K}$ and $\mathcal{V}$ are respectively the mean curvature and the normal velocity of Γ_t, taking the sign convention that the mean curvature of a sphere is positive and the normal velocity of an expanding hypersurface

is positive. In [8] one can find a deep study of this problem, namely classical solution's property of (4.1); the main result can be summarize as follows:

Theorem 4.0.1. *Assume that for some* $\alpha \in (0,1)$, $\Gamma_0 \in C^{3+\alpha}$. *Then there exist* $T > 0$ *such that* (4.1) *admits a unique solution satisfying* $\Gamma \in C^{3+\alpha,(3+\alpha)/3}$. *In addition, for every* $\tau \in (0,T)$, $\cup_{\tau \leq t \leq T}(\Gamma_t \times \{t\}) \in C^{\infty}$.

As one can see from the proof of the previous, Theorem 4.0.1 holds also for Dirichlet boundary conditions or mixed boundary conditions for u on $\partial\Omega \times [0,T]$. Other deep results, concerning weak solution of Eq. (4.1), can be found in [9].

Remark 4.0.2. We immediately notice that, although Problems (4.1) and (3.1) are related in some points, there is a huge difference: indeed in our coral's setting, the Laplace equation is solved at each time step in the complementary of the evolved coral and the velocity of the interface is due just to the gradient of the solution at the interface; on the other hand, in (4.1) the Laplace equation is solved in the whole domain (including the interior of the simulated coral) and the velocity of the interface is due to the sum of the inner and outward normal derivatives of the solution at the moving interface.

That's the reason why the previous theory cannot be adapted to the coral's PDE setting, at least not directly. A deep study of this point is thus required in order to understand the well posedness, uniqueness and existence, of (3.1); also, important questions about regularity of the evolved coral, either with or without surface tension effect, have to be answered. Of course, the same aspects can and must be studied for Eq. (3.6), where the effect of the fluid flow and the advection part are introduced in the coral's growth.

Moreover, in Chapter 3, a lot of numerical simulations of coral's growth are considered without taking into account the effect of the surface tension; the same work that we have done for the Mullins-Sekerka instability in Section 2.1, where we pointed out the convergence and the regularity effect due to this boundary condition, must be studied also in this case.

Furthermore may be also interesting to understand which aspect of the simulations are responsible for the growth of different coral's species; it is well known that about 6.000 different coral's species exist in the world. One can study in which particular conditions

this species growth and then transport this biological aspect in the PDE framework. It is essential to understand how complex morhogenesis can be and how this generates to a number of questions. However, we hope this work summarises the main aspects of the topic and sets out the foundations for future research.

Appendix A

PDEs tools

In order to understand the equations involved in the process, we provide a quick but rigorous presentation of them, including the study of the weak formultion so as to understand better the Finite Element Method setting used in FreeFem.

A.1 Linear functionals and bilinear forms: Lax-Milgram Theorem

Definition A.1.1. A functional F is a mapping (operator) from a set of functions $\mathcal{V}$ to the real space, i.e. $F : \mathcal{V} \to \mathbb{R}$. A functional is said to be *linear* if for each $v, w \in \mathcal{V}$ and $\alpha, \beta \in \mathbb{R}$:

$$F(\alpha v + \beta w) = \alpha F(v) + \beta F(w).$$

A functional is said to be *bounded* if:

$$|F(v)| \leq \Lambda \|v\|_{\mathcal{V}}.$$

Remark A.1.2. Bounded linear functionals are continuous. Indeed, given $v, w \in \mathcal{V}$ one has

$$\|F(v) - F(w)\|_{\mathcal{V}} = \|F(v - w)\|_{\mathcal{V}} \leq \Lambda \|v - w\|_{\mathcal{V}}.$$

Definition A.1.3. The set of all bounded linear functionals in $\mathcal{V}$ is called the *dual space*

of $\mathcal{V}$ and is denoted by $\mathcal{V}^*$; it is a Banach space with the norm given by:

$$\|F\|_{\mathcal{V}^*} = \sup_{v\in\mathcal{V}, v\neq 0} \frac{F(v)}{\|v\|_{\mathcal{V}}}.$$

Definition A.1.4. Given two normed function spaces $\mathcal{V}$ and $\mathcal{W}$, a bilinear form is a mapping from a pairs of functions $(v, w) \in \mathcal{V}\times\mathcal{W}$ and the real space, i.e. $a : \mathcal{V}\times\mathcal{W} \to \mathbb{R}$, that is linear separately in each of its two arguments.

Definition A.1.5. Let $\mathcal{V}$ and $\mathcal{W}$ be Hilbert spaces and $a : \mathcal{V} \times \mathcal{W} \to \mathbb{R}$ a bilinear form. We say that the bilinear form is

- *continuous* if there exist a constant $\gamma > 0$ s.t.

$$|a(u, v)| \leq \gamma \|u\|_{\mathcal{V}} \|v\|_{\mathcal{W}} \quad \forall\, u \in \mathcal{V},\, v \in \mathcal{W};$$

- *symmetric* if $\mathcal{V} = \mathcal{W}$ and for each $u, v \in \mathcal{V}$

$$a(u, v) = a(v, u);$$

- *coercive* if $\mathcal{V} = \mathcal{W}$ and there exist a constant $\alpha > 0$ such that

$$a(v, v) \geq \alpha \|v\|^2_{\mathcal{V}} \quad \forall\, v \in \mathcal{V}.$$

Remark A.1.6. Coercivity is fundamental to obtain a well-posed problem, as it states that the bilinear form is injective (has an empty kernel). But it is not only a theoretical property. Indeed it is the property that guarantees that the FEM system matrix can be inverted (is nonsingular) and the linear system can be solved.

We end this brief introduction stating the Lax-Milgram theorem; it is a fundamental result in order to guarantee uniqueness and well posedeness of the weak formulation of some PDEs.

Theorem A.1.7. *Let $a : \mathcal{V} \times \mathcal{V} \to \mathbb{R}$ a continuous and coercive bilinear form defined on an Hilbert space $\mathcal{V}$. For all bounded and continuous linear forms $F : \mathcal{V} \to \mathbb{R}$, there exists a unique function $u \in \mathcal{V}$ such that:*

$$a(u, v) = F(v) \quad \forall\, v \in \mathcal{V}.$$

A.2 Poisson equation

Let's consider one of the first equation introduced in the thesis, i.e., the Poisson equation

$$\begin{cases} -\mathrm{div}(D\,\nabla u) \,=\, f(x) \quad x \,\in\, \Omega \,\subset \mathbb{R}^d \\ u(x) \,=\, 0 \quad x \,\in\, \partial\Omega \end{cases} \tag{A.1}$$

where Ω is a bounded domain of $\mathbb{R}^d$ having boundary $\partial\Omega$ regular enough. We also assume that the diffusion coefficient $D \,\in\, L^{\infty}_{+}$, i.e., strictly greater than zero and integrable in Ω. Note that when $D = 1$ the equation reads

$$-\Delta u \,=\, f.$$

Let's now derive the weak formulation of (A.1); multiplying by a test function $v \,\in\, H^1_0(\Omega)$, integrating over Ω and using the Grenn's Lemma one obtains

$$a(u, v) \,=\, (f, v), \tag{A.2}$$

where

$$\begin{aligned} a(u, v) \,&=\, \int_{\Omega} D\,\nabla u \,\cdot\, \nabla v \,\mathrm{d}x \\ (f, v) \,&=\, \int_{\Omega} f\, v \,\mathrm{d}x. \end{aligned}$$

Remark A.2.1. Is quite easy to prove that:

- the solution of the weak problem is solution of the differential problem if u is sufficiently regular;
- the weak problem is equivalent to the following minimization problem: Find $u \,\in\, H^1_0(\Omega)$ such that

  $$F(u) \,\leq\, F(v) \quad \forall\, v \,\in\, H^1_0(\Omega),$$

  where

  $$F(v) \,=\, \frac{1}{2} a(v, v) \,-\, (f, v).$$

Moreover, thanks to the Lax-Milgram Theorem A.1.7, we know that, given $f \,\in\, L^2(\Omega)$, there exists a unique solution $u \,\in\, H^1_0(\Omega)$ of (A.2).

A.3 Stokes equation

In the case of a flow at low Reynolds number (for instance micro-organism) the Stokes equation holds, i.e.

$$-\mu\Delta\mathbf{u} + \nabla p = \mathbf{f} \quad \text{in } \Omega \tag{A.3}$$

$$\nabla \cdot \mathbf{u} = 0 \quad \text{in } \Omega \tag{A.4}$$

where $\mathbf{u} = (u_1, u_2)$ is the fluid velocity, p is the pressure and the positive constant μ can be seen as the viscosity coefficient of the fluid. In order to understand the procedure let's impose homogeneous Dirichlet Boundary conditions on the velocity, i.e. $\mathbf{u} = 0$ on the boundary $\Gamma := \partial\Omega$. Multipying by a test function $\mathbf{v} \in \mathbf{H}_0^1(\Omega) := [H_0^1(\Omega)]^2$ for (A.3) and $q \in L^2(\Omega)$ for (A.4), and applying integration by parts for the first equation we obtain the weak formulation of the Stokes equation: find $\mathbf{u} \in \mathbf{H}_0^1(\Omega)$ and a pressure $p \in L_0^2(\Omega)$ such that

$$\mu \int_\Omega \nabla\mathbf{u} : \nabla\mathbf{v} - \int_\Omega \mathrm{div}\mathbf{v}\, p = \int_\Omega \mathbf{f}\cdot\mathbf{v} \quad \forall\, \mathbf{v} \in \mathbf{H}_0^1(\Omega) \tag{A.5}$$

$$\int_\Omega \mathrm{div}\mathbf{u}\, q = 0 \quad \forall\, q \in L_0^2(\Omega). \tag{A.6}$$

where

$$L_0^2 = \left\{ q \in L^2(\Omega) : \int_\Omega q \, \mathrm{d}x = 0 \right\}.$$

Remark A.3.1. A natural choise of the pressure space is $L_0^2(\Omega)$. Note that

$$\int_\Omega \mathrm{div}\,\mathbf{v}\,\mathrm{d}\mathbf{x} = \int_{\partial\Omega} \mathbf{v}\cdot\mathbf{n} dS = 0$$

due to the boundary condition. Thus div operator will map $H_0^1(\Omega)$ into the subspace $L_0^2(\Omega)$, in which the pressure solving the Stokes equations is unique. In $L^2(\Omega)$ is unique only up to a constant.

The two equations (A.5)-(A.6) can be rewritten in a more compact form, i.e. find $(\mathbf{u}, p) \in \mathbf{H}_0^1(\Omega) \times L_0^2(\Omega)$ s.t.

$$\begin{cases} a(\mathbf{u}, v) + b(\mathbf{v}, p) = (\mathbf{f}, \mathbf{v}) \\ b(\mathbf{u}, q) = 0 \end{cases} \tag{A.7}$$

for all $(\mathbf{v}, q) \in \mathbf{H}_0^1(\Omega) \times L^2(\Omega)$. In particular

$$a(\mathbf{u}, v) = \mu \int_\Omega \nabla \mathbf{u} : \nabla \mathbf{v}$$
$$b(\mathbf{u}, q) = -\int_\Omega \mathrm{div}\mathbf{u}\, q.$$

A.3.1 Penalty method

This method is actually used in FreeFem in order to solve Stokes equation. It consist of replacing A.7 by a more regular problem: find $(\mathbf{u}^\varepsilon, p^\varepsilon) \in \mathbf{H}_0^1(\Omega) \times L_0^2(\Omega)$ s.t.

$$a(\mathbf{u}^\varepsilon, v) + b(\mathbf{v}, p^\varepsilon) = (\mathbf{f}, \mathbf{v}) \tag{A.8}$$
$$b(\mathbf{u}^\varepsilon, q) - \varepsilon(p^\varepsilon, q) = 0 \tag{A.9}$$

for all $(\mathbf{v}, q) \in \mathbf{H}_0^1(\Omega) \times L^2(\Omega)$. Formally we have

$$\mathrm{div}(\mathbf{u}^\varepsilon) = \varepsilon p^\varepsilon.$$

A.4 Navier-Stokes Equation

Let $\Omega \subset \mathbb{R}^d$, $d \leq 2$, denote the bounded and connected domain under investigation. The Navier-Stokes equations can be written as:

$$\rho \frac{\partial \mathbf{u}}{\partial t} - 2\mathrm{div}(\mu \mathbf{D}(\mathbf{u})) + \rho(\mathbf{u} \cdot \nabla)\mathbf{u} + \nabla p = \mathbf{0}, \quad \text{in } \Omega \times I \tag{A.10}$$
$$\mathrm{div}\mathbf{u} = 0, \quad \text{in } \Omega \times I \tag{A.11}$$

where $I = (0, T]$ is the time interval, $\mathbf{u}$ and p are the velocity vector field and scalar pressure of the fluid, ρ and μ are the density and the dynamic viscosity of the fluid, respectively, and $\mathbf{D}(\mathbf{u})$ is the linear fluid deformation tensor (given by the expression $\frac{1}{2}(\nabla \mathbf{u} + \nabla \mathbf{u}^T)$). Recall moreover the following notation

$$(\mathbf{u} \cdot \nabla)\mathbf{u} = \begin{bmatrix} \sum_{i=1}^{d} u_i \partial_{x_i} u_1 \\ \vdots \\ \sum_{i=1}^{d} u_i \partial_{x_i} u_d \end{bmatrix}$$

These notations allow us to define the stress tensor $\sigma(\mathbf{u}, p) = -p\mathbf{I} + 2\mu\mathbf{D}(\mathbf{u})$, where $\mathbf{I}$ is the identity tensor. The system (A.10) - (A.11) is completed with appropiate initial and boundary conditions that will be detailed later. The flow is characterized by the Reynolds number:

$$Re = \frac{\rho DU}{\mu}, \tag{A.12}$$

a dimensionless number that identifies the transition of the flow to turbulence. It depends on a characteristic linear dimension D, the mean velocity U, the density and the viscosity of the fluid. The higher the Reynolds number gets, the more turbolent the flow becomes, and vice-versa.

Variational form of the Navier-Stokes equations

To write formally a variational formulation of the problem (A.10) - (A.11), let us denote by $\mathbb{V}$ and $\mathbb{M}$ the functional spaces for the velocity and pressure fields, respectively. These spaces will be set later according to the specific choises of boundary conditions. We will take, for the moment, $\mathbb{V} = [H^1(\Omega)]^d$ and $\mathbb{M} = L^2(\Omega)$.
Taking the scalar product of equation (A.10) by a test function $\mathbf{v} \in \mathbb{V}$, multiplying equation (A.11) by a test function $q \in \mathbb{M}$, integrating the resulting equalities over Ω, we are led to the following weak formulation: for every $t > 0$, find $(\mathbf{u}(t), p(t)) \in \mathbb{V} \times \mathbb{M}$ such that $\forall\, \mathbf{v} \in \mathbb{V}$, $\forall\, q \in \mathbb{M}$,

$$\int_\Omega \rho \frac{\partial \mathbf{u}}{\partial t}\mathbf{v}\,\mathrm{d}\mathbf{x} + \int_\Omega \rho(\mathbf{u}(t)\cdot\nabla)\mathbf{u}(t)\cdot\mathbf{v}\,\mathrm{d}\mathbf{x} - 2\mu\int_\Omega \mathrm{div}(\mathbf{D}(\mathbf{u}(t)))\cdot\mathbf{v}\,\mathrm{d}\mathbf{x} + \int_\Omega \nabla p(t)\cdot\mathbf{v}\,\mathrm{d}\mathbf{x} = 0,$$
$$\int_\Omega q\,\mathrm{div}(\mathbf{u}(t))\,\mathrm{d}\mathbf{x} = 0.$$

Integrating by parts the third and fourth integrals of the previous equation we obtain the weak formulation, i.e. for every $t > 0$, find $(\mathbf{u}(t), p(t)) \in \mathbb{V} \times \mathbb{M}$ such that $\forall\, \mathbf{v} \in$

$\mathbb{V}$, $\forall\, q \in \mathbb{M}$,

$$\int_\Omega \rho \frac{\partial \mathbf{u}}{\partial t}\mathbf{v}\,\mathrm{d}\mathbf{x} + \int_\Omega \rho(\mathbf{u}\cdot\nabla)\mathbf{u}\cdot\mathbf{v}\,\mathrm{d}\mathbf{x} + 2\mu\int_\Omega \mathbf{D}(\mathbf{u}) : \nabla\mathbf{v}\,\mathrm{d}\mathbf{x} - 2\mu\int_{\partial\Omega}\mathbf{D}(\mathbf{u})\mathbf{n}\cdot\mathbf{v}\,\mathrm{d}s + \int_{\partial\Omega} p\mathbf{v}\cdot\mathbf{n}\,\mathrm{d}s - \int_\Omega p\,\mathrm{div}(\mathbf{v})\,\mathrm{d}\mathbf{x} = 0,$$
$$\int_\Omega q\,\mathrm{div}(\mathbf{u})\,\mathrm{d}\mathbf{x} = 0.$$

Equivantly, using the stress tensor: find $(\mathbf{u}, p) \in \mathbb{V}\times\mathbb{M}$ such that $\forall\,\mathbf{v}\in\mathbb{V}$, $\forall\, q \in \mathbb{M}$

$$\int_\Omega \rho \frac{\partial \mathbf{u}}{\partial t}\mathbf{v}\,\mathrm{d}\mathbf{x} + \int_\Omega \rho(\mathbf{u}\cdot\nabla)\mathbf{u}\cdot\mathbf{v}\,\mathrm{d}\mathbf{x} + 2\mu\int_\Omega \mathbf{D}(\mathbf{u}) : \nabla\mathbf{v}\,\mathrm{d}\mathbf{x} - \int_{\partial\Omega}\sigma(\mathbf{u},p)\mathbf{n}\cdot\mathbf{v}\,\mathrm{d}s - \int_\Omega p\,\mathrm{div}(\mathbf{v})\,\mathrm{d}\mathbf{x} = 0, \quad \text{(A.13)}$$
$$\int_\Omega q\,\mathrm{div}(\mathbf{u})\,\mathrm{d}\mathbf{x} = 0. \quad \text{(A.14)}$$

We have not yet incorporated the boundary conditions in the weak formulation. To do so, let us start with denoting $\partial\Omega = \Gamma_{\text{in}} \cup \Gamma_{\text{out}} \cup \Gamma_{\text{w}}$ the local Lipschitz boundary of the domain Ω where Γ_{w} is the wall where we consider an adherence boundary condition, Γ_{in} the inlet and Γ_{out} the outlet of a chanel. The common boundary condition to all our following simulations is the *no slip* condition on Γ_{w}, i.e.

$$\mathbf{u} = \mathbf{0} \ \text{ on } \ \Gamma_{\text{w}}. \quad \text{(A.15)}$$

The standard manner to deal with this essential boundary condition is to choose the functional space $\mathbb{V}$ as

$$\mathbb{V} = \{\mathbf{v} \in [H^1(\Omega)]^d \,|\, \mathbf{v} = \mathbf{0} \ \text{ on } \ \Gamma_{\text{w}}\}. \quad \text{(A.16)}$$

Within this functional setting for the velocity field, equations (A.13) - (A.14) are rewritten as: find $(\mathbf{u}, p) \in \mathbb{V}\times\mathbb{M}$ such that $\forall\,\mathbf{v}\in\mathbb{V}$, $\forall\, q \in \mathbb{M}$

$$\int_\Omega \rho \frac{\partial \mathbf{u}}{\partial t}\mathbf{v}\,\mathrm{d}\mathbf{x} + \int_\Omega \rho(\mathbf{u}\cdot\nabla)\mathbf{u}\cdot\mathbf{v}\,\mathrm{d}\mathbf{x} + 2\mu\int_\Omega \mathbf{D}(\mathbf{u}) : \nabla\mathbf{v}\,\mathrm{d}\mathbf{x} - \int_{\Gamma_{\text{in}}\cup\Gamma_{\text{out}}}\sigma(\mathbf{u},p)\mathbf{n}\cdot\mathbf{v}\,\mathrm{d}s - \int_\Omega p\,\mathrm{div}(\mathbf{v})\,\mathrm{d}\mathbf{x} = 0, \quad \text{(A.17)}$$
$$\int_\Omega q\,\mathrm{div}(\mathbf{u})\,\mathrm{d}\mathbf{x} = 0. \quad \text{(A.18)}$$

In the weak formulation (A.17) - (A.18), we have to take into account the boundary conditions on the inlet and outlet parts of the boundary. It is very important to choose this boundary conditions in a proper way in order not to change the physics of the problem.

Boundary conditions

There are several way to impose the boundary conditions. One of the classical boundary conditions occurs when we know the velocity profiles at inlets and outlets. This *Dirichlet - Dirichlet* buondary conditions do not corresponds to the most common real situation because, in general, we do not know exactly the velocity profile at the outlet sections, even if we know it at the inlets. Indeed it is difficult to predict the velocity profile at outlets since it depends on the channel geometry or the number of outlets sections etc... . Therefore we can consider the so-called *Dirichlet - Neumann* boundary conditions. These boundary conditions can be formalized as

$$\mathbf{u} = \mathbf{u}_{\text{in}} \qquad \text{on } \Gamma_{\text{in}} \tag{A.19}$$

$$\sigma(\mathbf{u}, p)\,\mathbf{n} = \mathbf{g}_N \qquad \text{on } \Gamma_{\text{out}} \tag{A.20}$$

In this case we have the following variational formulation: find $(\mathbf{u}, p) \in \mathbb{V} \times \mathbb{M}$ such that $\forall\, \mathbf{v} \in \{\mathbf{v} \in [H^1(\Omega)]^d \,|\, \mathbf{v} = \mathbf{0} \text{ on } \Gamma_{\text{w}} \cup \Gamma_{\text{in}}\}.$, $\forall\, q \in \mathbb{M}$

$$\int_\Omega \rho \frac{\partial \mathbf{u}}{\partial t}\mathbf{v}\,\mathrm{d}\mathbf{x} + \int_\Omega \rho(\mathbf{u}\cdot\nabla)\mathbf{u}\cdot\mathbf{v}\,\mathrm{d}\mathbf{x} + 2\mu\int_\Omega \mathbf{D}(\mathbf{u}) : \nabla\mathbf{v}\,\mathrm{d}\mathbf{x} - \int_{\Gamma_{\text{out}}} \mathbf{g}_N\cdot\mathbf{v}\,\mathrm{d}s$$
$$- \int_\Omega p\,\mathrm{div}(\mathbf{v})\,\mathrm{d}\mathbf{x} = 0, \tag{A.21}$$

$$\int_\Omega q\,\mathrm{div}(\mathbf{u})\,\mathrm{d}\mathbf{x} = 0. \tag{A.22}$$

with

$$\mathbf{V} = \{\mathbf{v} \in [H^1(\Omega)]^d \,|\, \mathbf{v} = \mathbf{0} \text{ on } \Gamma_{\text{w}},\ \mathbf{v} = \mathbf{u}_{\text{in}} \text{ on } \Gamma_{\text{in}}\} \text{ and } \mathbf{M} = L^2_0(\Omega). \tag{A.23}$$

When at the outlet the viscous stress is set to zero, i.e. $\mathbf{g}_N = \mathbf{0}$, the weak equations

read:

$$\int_\Omega \rho \frac{\partial \mathbf{u}}{\partial t} \mathbf{v} \, \mathrm{d}\mathbf{x} + \int_\Omega \rho (\mathbf{u} \cdot \nabla) \mathbf{u} \cdot \mathbf{v} \, \mathrm{d}\mathbf{x} + 2\mu \int_\Omega \mathbf{D}(\mathbf{u}) \, : \, \nabla \mathbf{v} \, \mathrm{d}\mathbf{x} - \int_\Omega p \, \mathrm{div}(\mathbf{v}) \, \mathrm{d}\mathbf{x} \, = \, 0, \tag{A.24}$$

$$\int_\Omega q \, \mathrm{div}(\mathbf{u}) \, \mathrm{d}\mathbf{x} \, = \, 0. \tag{A.25}$$

This conditions describe boundaries that are open to large volumes of fluid, which is free to enter or leave the simulation domain.

A.5 Finite Element Method

All the codes that have been implemented use the variational formulation of PDEs from the mathematical point of view and always the *Finite Element Method* from the numerical point of view. Our aim in this section is to introduce the preceding method in order to understand the main ideas associated to it; indeed FreeFem software hides the features of the method, underlying just the variational formulation of the equations; it is thus important to use all the advantages of the FreeFem software, without forget the numerical method behind it. In order to present the FEM method we will focus on a quite general setting for elliptic equations. Of course this remains just a quick overview of the FEM method. There are also important results concerning convergence of the method and all the literature of FEM for parabolic equations that will not be trated in the following pages. All of these informations can be found in [3].

A.5.1 Abastract formulation of the FEM for elliptic equations

Let us consider a generic Hilbert space $\mathcal{V}$ equipped with scalar product $(\cdot, \cdot)_\mathcal{V}$ and norm $\|\cdot\|_\mathcal{V}$. Denote with $a : \mathcal{V} \times \mathcal{V} \to \mathbb{R}$ a continuous and coercive bilinear form and with $F : \mathcal{V} \to \mathbb{R}$ a continuous linear form, i.e. $F \in \mathcal{V}'$, the dual space of $\mathcal{V}$. The weak (variational) formulation of the problem reads: Find $u \in \mathcal{V}$ such that

$$a(u, v) \, = \, F(v) \quad \forall \, v \, \in \, \mathcal{V}. \tag{A.26}$$

We observed that continuity and coericivity of the bilinear form, together with continuity of the linear form defined by the source term, are the key ingredients to guarantee existence and uniqueness of the solution of the variational problem, thanks to Theorem A.1.7. These properties will play an importnat role also in the discrete setting and will guarantee convergence if the FEM spaces are chosen appropiately. However there are problems where the bilinear form is not coercive and we need some weaker statement. This condition is called *inf-sup* or *LBB* condition.

The FEM formulation is obtained by approximating the appriopate functional space with a finite-dimensionale subset $\mathcal{V}_h \subset \mathcal{V}$ generated by a finite number of basis function $\{\phi_1, \dots, \phi_n\}$. Then, every function $v \in \mathcal{V}_h$ can be written as

$$v = \sum_{i=1}^{n} \xi_i \, \phi_i(x). \tag{A.27}$$

Hence Problem A.26 reads: Find $u_h \in \mathcal{V}_h$ such that

$$a(u_h, v) = F(v) \quad \forall \, v \in \mathcal{V}_h. \tag{A.28}$$

Using the representation of u_h as linear combination of ϕ_i

$$u = \sum_{j=1}^{n} u_j \, \phi_j(x).$$

we obtain:

$$\sum_{j=1}^{n} u_j \, a(\phi_j, \phi_i) = F(\phi_i), \qquad i = 1, \dots n,$$

or, in matrix form,

$$Au = b, \tag{A.29}$$

where $u = \{u_i\}$, $A = \{a_{i,j}\}$, $a_{i,j} = a(\phi_i, \phi_j)$, $b = \{b_i\}$. Matrix A is called the *Stiffness matrix*. Using simmetry and coercivity of the bilinear form a, it is easy to prove that A is simmetric and positive definite, which ensure that the system (A.29) has a unique solution.

Suppose now that $\mathcal{V} = H^1(\Omega)$. To complete the theory of finite element space we need to build the space $\mathcal{V}_h$, i.e. we need to construct the set of basis functions $\{\phi_i(x)\}$ that span $\mathcal{V}_h \subset H^1(\Omega)$. Obviously we need to build linear system that are easy to solve numerically.

The FEM choise is to arrive at large sparse matrices, for which efficient solvers exist. This can be achieved by means piecewise polynomials defined on appropiate subdivision of the domain $\Omega \subset \mathbb{R}^d$, called generally triangulation. A triangulation $\mathcal{T}_h = \{T\}$ is formed by the union of non-overlapping elements T that form Ω without intersections. This allows to work element by element basis, i.e., construct elementwise $\phi_i^{(T)}(x)$ that glue appropiately at the element boundary in such a way that the global function has the proper continuity properties. (in Figure A.1 one can see an example of admissible triangulation and linear basis functions).

Let the domain $\Omega \subset \mathbb{R}^2$ be chracterized by a polygonal boundary Γ. Let $\mathcal{T}_h = \{T\}$ be

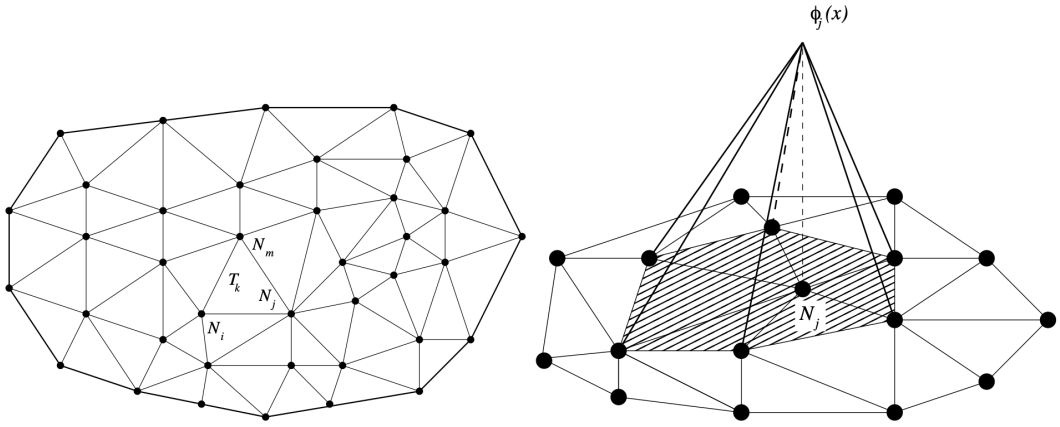

Figure A.1: Left: Example of admissible triangulation of Ω. Right: Linear (pyramidal) basis function $\phi_j(x) \in \mathcal{V}_h$.

a triangulation formed by triangular elements T, and let $\mathcal{P}_r(T)$ be the set of polynomials of degree at most r in T. A linar polynomial $v \in \mathcal{P}_1(T)$ can be written as

$$v(x) = a_{00} + a_{10}x_1 + a_{01}x_2, \;\; x \in T,$$

with $a_{ij} \in \mathbb{R}$. For instance, one can define affine polynomials on the triangles (Figure A.2), i.e.

$$\mathcal{V}_h = \{v \in C^0(\overline{\Omega}) : v|_T \in \mathcal{P}_1(T) \, \forall \, T \in \mathcal{T}_h\}.$$

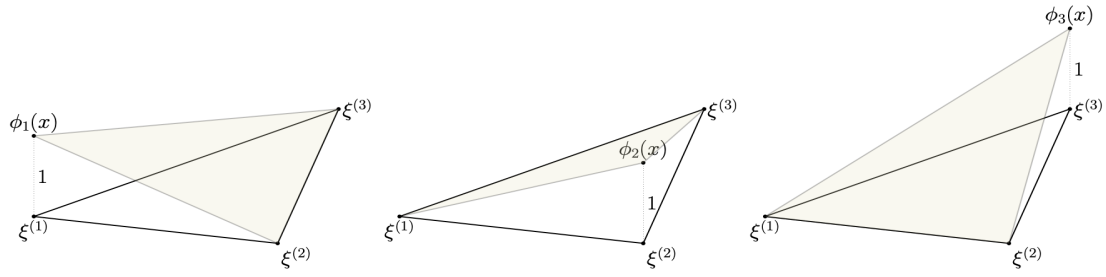

Figure A.2: Example of linear basis functions

This space is formed by functions that are piecewise linear with derivatives that are piecewise constant. To describe these functions we use the *degrees of freedom*, in this case the nodes of $\mathcal{T}_h$. Every function $v \in \mathcal{V}_h(T)$ is uniquely determined by its values at the nodes of T, namely $\alpha_i \in \mathbb{R}$, $i = 1, 2, 3$. Then, following the Lagrangian interpolation idea, we can choose α_i equal to $(1, 0, 0)$, $(0, 1, 0)$, $(0, 0, 1)$. In this way it is easy to see that

- $\phi_k^{(T)}(x)$ assumes nonzero values only inside the element T;
- $\phi_k^{(T)}(x) = 1$ on one node and zero on the other two nodes.

The same idea holds for quadratic basis function; in this case the space $\mathcal{V}_h$ is given by

$$\mathcal{V}_h = \{v \in C^0(\overline{\Omega}) : v|_T \in \mathcal{P}_2(T) \, \forall \, T \in \mathcal{T}_h\}.$$

To describe these functions we need six degrees of freedom $T \in \mathcal{T}_h$. We choose the vertices of T and the midpoints of each edge (Figure A.3).

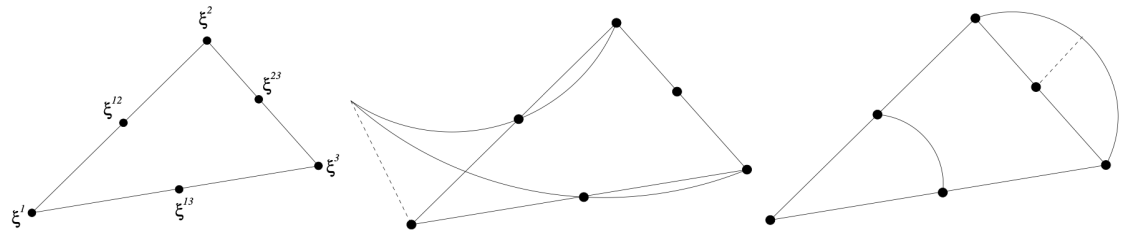

Figure A.3: Example of quadratic basis functions

Remark A.5.1. Usually the previous spaces of linear and quadratic polynomials are referred in literature as P1/P2 - Galerkin space.

Appendix B

Random Walk

As we have seen in Section 1.3, the main connection between DLA and Laplacian growth lies in the description of the random walk, and its connection with the PDE framework. The aim of this appendix is to briefly introduce the random walk and explain why the probability density is connected with the heat equation. For more details about the random walk in its generality, one can see [7].

B.1 Simmetric Random Walk and Diffusion Processes

In order to understand the main features of the random walk, we start with the basic case, i.e., the symmetric random walk in dimension one. Let's consider a unit mass particle that moves randomly along the x axis, according to the following rules:

- fix a space step $h > 0$ and a time interval τ;
- the particle start from the position $x = 0$ at the time $t = 0$;
- during an interval of time τ, the particle takes one step of h unit lenght from the previous position;
- The particle moves to the left or to the right with probability $p = \frac{1}{2}$, independently from the previous step.

At time $t = N\tau$, after N steps, the particle will be at a point $x = mh$, where $N \geq 0$ and m are integers, $-N \leq m \leq N$. We are interested in getting the probability density of the location of the particle $u(x,t)$ that is, the probability of finding the particle inside the interval $[a,b]$ at time t is

$$\int_a^b u(x,t)\,\mathrm{d}x,$$

as the time/space steps $h, \tau \searrow 0$. In order to do this we can obtain a differential equation satisfied by studying the relation between $u(x,t)$ at an earlier and a later time.
Consider the probability of the particle reaching location x at time $t+\tau$. According to the rules of the motion, there are only two possibilities: the particle was at $x-h$ at time t, and jumped to the right; or the particle was at $x+h$ at time t and jumped to the left. As the location of the particle at time t and the direction of its next movement are independent, the first situation happens with probability $\frac{1}{2}u(x-h,t)$ while the second with $\frac{1}{2}u(x+h,t)$. Therefore

$$u(x,t+\tau) = \frac{1}{2}u(x+h,t) + \frac{1}{2}u(x-h,t). \tag{B.1}$$

with the initial conditions

$$u(0,0) = 1 \qquad \text{and} \qquad u(x,0) = 0 \text{ if } x \neq 0.$$

Let us suppose that $u(x,t)$ is C^2 w.r.t. x and C^1 w.r.t. t. Using Taylor's formula we can write

$$u(x,t+\tau) = u(x,t) + \tau\,\partial_t u(x,t) + o(\tau),$$
$$u(x \pm h,t) = u(x,t) \pm h\,\partial_x u(x,t) + h^2\,\frac{1}{2}\,\partial_{x,x}u(x,t) + o(h^2).$$

Substituting into (B.1) we have

$$\begin{aligned} u(x,t) + \tau\,\partial_t u(x,t) + o(\tau) = {} & \frac{1}{2}[u(x,t) + h\,\partial_x u(x,t) + h^2\,\frac{1}{2}\,\partial_{x,x}u(x,t) + o(h^2)] \\ & + \frac{1}{2}[u(x,t) - h\,\partial_x u(x,t) + h^2\,\frac{1}{2}\,\partial_{x,x}u(x,t) + o(h^2)]. \end{aligned}$$

Thus

$$\tau\,\partial_t u(x,t) + o(\tau) = \frac{h^2}{2}\,\partial_{x,x}u(x,t) + o(h^2).$$

Dividing both sides by τ,

$$\partial_t u(x,t) + o(1) = \frac{h^2}{2\tau}\,\partial_{x,x} u(x,t) + o\left(\frac{h^2}{\tau}\right).$$

Now we see that nontrivial dynamics only happpen when $\frac{h^2}{\tau} \to 2D$ for some positive and finite D. Passing to the limit we get for u the equation

$$\partial_t u(x,t) = D\partial_{x,x} u(x,t) \;\text{ with }\; \lim_{t\to 0^+} u(x,t) \;=\; \delta. \tag{B.2}$$

From the standard PDE's theory the unique solution of (B.2) is

$$u(x,t) \;=\; \Phi_{1,D}(x,t) = \frac{1}{(4\pi D t)^{\frac{1}{2}}} e^{-\frac{|x|^2}{4Dt}}$$

since

$$\int_{\mathbb{R}} u(x,t)dx \;=\; 1.$$

Of course one can easily pass from the 1D-case to the multidimensional random walk. To define a symmetric random walk, we introduce the lattice $\mathbb{Z}^n$ given by the set of points $x \in \mathbb{R}^n$, whose coordinates are signed integers. Given the space step $h > 0$, the symbol $h\mathbb{Z}^n$ denotes the lattice of points whose coordinates are signed integers multiplied by h. Every point $\mathbf{x} \in h\mathbb{Z}^n$, has a "discrete neighborhood" of $2n$ points at distance h, given by

$$\mathbf{x} + h\mathbf{e}_j, \quad \mathbf{x} - h\mathbf{e}_j \quad (j = 1, \ldots, n),$$

where $\mathbf{e}_1, \ldots, \mathbf{e}_n$ is the canonical basis in $\mathbb{R}^n$. Our particle moves in $h\mathbb{Z}^n$ according to the same rules of the 1D case, i.e.,

- the particle start from the position $\mathbf{x} = 0$ at the time $t = 0$;
- If it is located in $\mathbf{x}$ at time t, at time $t + \tau$ the particle location is at one of the $2n$ points $\mathbf{x} \pm h\mathbf{e}_j$,with probability $p = \frac{1}{2n}$;
- Each step is independent of the previous one.

As the 1D-case, our task is to compute the probability density $u(\mathbf{x}, t)$ of finding the particle in $\mathbf{x}$ at time t. Equation (B.1) easily extends in the multidimensional case, namely:

$$u(\mathbf{x}, t+\tau) \;=\; \frac{1}{2n}\sum_{j=1}^{n} \{p(\mathbf{x} + h\mathbf{e}_j, t) \;+\; p(\mathbf{x} - h\mathbf{e}_j, t)\}. \tag{B.3}$$

Using the same idea of the 1D-case, assuming enough regularity of u and using Taylor's formula we arrive to the n-dimensional heat equation

$$\partial_t u \;=\; D\,\Delta u \tag{B.4}$$

with the initial condition

$$\lim_{t\to 0^+} u(\mathbf{x},t) \;=\; \delta,$$

where we have supposed that $\frac{h^2}{\tau} \to 2nD$. Again the unique solution of (B.4) is

$$u(\mathbf{x},t) \;=\; \Phi_{n,D}(\mathbf{x},t) = \frac{1}{(4\pi D t)^{\frac{n}{2}}} e^{-\frac{|\mathbf{x}|^2}{4Dt}}$$

since

$$\int_{\mathbb{R}^n} u(\mathbf{x},t)d\mathbf{x} \;=\; 1.$$

Remark B.1.1. Returning to DLA and Section 1.3 we can understand the importance of the following assumption made when we introduced the DLA algorithm: we supposed that the density of the colloidal particles was quite low, so one could imagine that the aggregation process occured one particle at a time. This allows us to consider a quasi-stationary process and that's the reason why the PDE satisfied by the probability density out of the cluster is not the heat equation, but simply the Laplace equation $\Delta u = 0$, as we expected from the stochastic version of the Laplacian Growth.

Appendix C

Codes

C.1 Mullin-Sekerka's Instability

Here we provide the FreeFem code used in order to verify numerically the Mullin-Sekerka's instability presented in Section 2.1.1. Both boundary conditions, with and withouth surface tension, are included in the code.

```
1  /*
2
3    Mullins–Sekerka instability on a 2D circle: Laplacian growth performed on a slightly
       ↪ deformed circle;
4    Surface tension is added to the code in order to see convergence of the method.
5
6    May 2022.
7
8    Mauro D'Annibale & Emmanuel Dormy
9
10 */
11
12
13 load "Curvature"
14 load "isoline"
```

```
15
16 real eps = 0.09;
17 int m = 3;
18 real dt=0.1;
19 int Niter = 250;
20 real r0 = 1.2;
21 real cap=0.02; // >= 0.01 otherwise is too small
22 real dtMax = 0.1; // Maximum dt
23 real CFL = 0.5; //CFL condition 0 < CFL < 1
24 int n = 100;
25 int zoom = 12;
26 real size = 0.2; //Vary the size of the triangles in order to see the differences between
       ↪ BCs
27
28 //Define the domain
29 border a(t=0, 2*pi){x=10*cos(t); y=10*sin(t); label=1;}
30 border b(t=0, 2*pi){x=(r0+eps*cos(m*t))*cos(t); y=(r0+eps*cos(m*t))*sin(t); label
       ↪ =2;}
31
32 //plot(a(200) + b(-300)); //to see a plot of the border mesh
33 mesh Th = buildmesh(a(n) + b(-2*n),fixedborder=true); // mesh with the desired
       ↪ hole
34
35 //Finite element spaces
36 fespace Vh(Th, P1);
37 fespace Ch(Th, P1); // Auxiliary function to move the interface
38 fespace Hh (Th, P0); // Size of the triangles
39 Hh h = hTriangle;
40 Vh u, v, c, g;
41
42 // Loop
```

```
43 for (int iter=0 ; iter<Niter ; iter++) {
44         //Compute the curvature
45         c = 0;
46         c[] = curvature(Th,2);
47         g = -c*cap;
48
49     // Poisson solution
50         solve Poisson(u, v, solver=LU)
51         = int2d(Th)(
52                             (
53                   dx(u)*dx(v)
54                 + dy(u)*dy(v))
55                  )
56                   //+ on(2, u= 0) //boundary condition without surface tension
57                   + on(2, u = g) //boundary condition with surface tension
58                   + on(1, u = 1)
59         ;
60
61         // Auxilary variable to prevent memory leaks
62         real[int] tmp(u[].n);
63
64         // Compute the partial derivatives
65     Hh dxu = dx(u);
66     Hh dyu = dy(u);
67
68         //Plot the evolved mesh
69         plot(Th,[dxu,dyu], wait=0, fill=false,value=true,bb=[[-zoom, -zoom], [zoom,
               ↪ zoom]]);
70
71     // Compute the new dt with CFL condition
72         h = hTriangle;
```

```
73      real hMin = h[].min;
74      real dxumax = dxu[].max;
75      real dyumax = dyu[].max;
76      real dumax = max(dxumax,dyumax);
77          dt = min(dtMax,CFL*hMin/dumax);
78
79      // Movemesh
80          Th = movemesh(Th, [x+dt*dxu, y+dt*dyu]);
81
82          Save the last iteration
83          if (iter == Niter-1){
84          plot(Th,[dxu,dyu], wait=0, fill=false,value=false,bb=[[-zoom, -zoom], [zoom,
                ↪ zoom]], ps="Mullins-Sekerka-curv_3.eps");
85      }
86
87      // To prevent memory leaks
88      tmp = u[]; //save the value
89      u = 0;//to change the FEspace and mesh associated with u
90      h=0;
91      u[] = tmp;//set the value of u without any mesh update
92      v=0; g=0; dxu=0; dyu=0;
93
94      // Adapt mesh
95      Th = adaptmesh(Th,u,hmax=size,hmin=size);
96
97  }
```

C.2 2D Coral's Growth

Here we provide the FreeFem code used in order to solve the free boundary problem (3.1) in Section 3.1 (both boundary conditions can be implemented easily).

```
/*

  Simulation of a Coral growth under a Laplacian growth

  May 2022.

  Mauro D'Annibale & Emmanuel Dormy

*/

  // Simulation parameters
  real dt =0.01;
  int Niter = 500;
  int n = 50;
  real C0 = 10;
  real r0 = 0.2;
  real CFL = 0.5; //CFL condition, 0<CFL<1
  real dtMax = 0.1;

  // Building the initial mesh
  border C01(t=0, 1){x=3*t; y=0; label=1;}
  border C02(t=0, 1){x=3; y=2*t; label=2;}
  border C03(t=0, 1){x=3*(1-t); y=2; label=3;}
  border C04(t=0, 1){x=0; y=2*(1-t); label=4;}
  border C05(t=0, 2*pi){x=1.5 + r0*cos(t); y=r0 + r0*sin(t); label=5;}

  //Define the initial mesh
  mesh Th = buildmesh(C01(n) + C02(n) + C03(n)+ C04(n) + C05(-2*n) ,
      ↪ fixedborder=true);

  //Finite element space
```

```
31  fespace Vh(Th, P1);
32  fespace Ch(Th, P1); // Auxiliary function to move the interface
33  fespace Hh (Th, P0); // Size of the triangles
34  Vh u, v; // Define u and v as piecewise-P1 continuous functions
35  Ch cxu,cyu,tcx,tcy;
36  Hh h = hTriangle;
37
38  //Poisson problem
39  problem Poisson(u, v, solver=LU)
40  = int2d(Th)( // The bilinear part
41                (
42                        dx(u)*dx(v)
43            + dy(u)*dy(v))
44                    )
45  + on(1,5, u=0) //boundary conditions
46  + on(2,3,4, u=10) //Dirichlet boundary conditions
47  //+ on(3, u=10) //Noflux boundary conditions
48  ;
49
50  // Problem to transport the interface
51  problem MeshVeloc([cxu,cyu],[tcx,tcy])=
52          int2d(Th)(
53              2*dx(cxu)*dx(tcx)
54            + 2*dy(cyu)*dy(tcy)
55            + dx(cyu)*dx(tcy)
56            + dy(cxu)*dy(tcx)
57            + dx(cyu)*dy(tcx)
58            + dy(cxu)*dx(tcy)
59                                    )
60                    + int1d(Th,5)(
61                (tcy*cyu+tcx*cxu)*0.0001
```

```
62                          )
63
64          + on(1,2,3,4,cxu=0,cyu=0)
65          + on(5,cxu=dx(u),cyu=dy(u))
66  ;
67
68
69    //Loop
70    for (int iter=0 ; iter<Niter ; iter++) {
71
72    //Solve Poisson equation
73    Poisson;
74
75    // Plot the solution and the changed mesh
76    plot(Th,u, fill=true,wait=0,ps="Coral2D_BC1.eps");
77
78    //Compute the mesh velocity vector field
79    MeshVeloc;
80
81    // To prevent memory leaks
82    real[int] tmp(u[].n);
83    real[int] tmpc(cxu[].n);
84
85    // Compute the new dt with CFL condition
86    h = hTriangle;
87    real hMin = h[].min;
88    real cxumax = cxu[].max;
89    real cyumax = cyu[].max;
90    real cmax = max(cxumax,cyumax);
91    dt = min(dtMax,CFL*hMin/cmax);
92
```

```
93      // Movemesh
94      Th = movemesh(Th, [x+dt*(cxu), y+dt*(cyu)]);
95
96      // Prevent memory leaks
97      tmp = u[]; //save the value
98      u = 0;//to change the FEspace and mesh associated with u
99      u[] = tmp;//set the value of u without any mesh update
100     h=0;
101     tmpc=cxu[]; cxu=0; cxu[]=tmpc ;
102     tmpc=cyu[]; cyu=0; cyu[]=tmpc ;
103     tcx = 0; tcy = 0; v=0;
104
105     // Adapt the mesh
106     Th = adaptmesh(Th, 1./50, IsMetric=1, nbvx=10000);
107
108 }
```

Bibliography

[1] W.W. Mullinks and R.F. Sekerka, *Morphological stability of a Particle Growing by Diffusion or Heat Flow*. J. Appl. Phys. Chem 34, 323 (1963).

[2] Bodil Oust, *Laplacian growth patterns: a study of boundary evolution using iterated conformal maps and Loewner evolution*. Thesis submitted for the degree Master of Science. (2009).

[3] Mario Putti, Antonia Larese, *Notes on Numerical Methods for Differential Equations*, Department of Mathematics "Tullio Levi-Civita"– University of Padua

[4] Chindapol N, Kaandorp JA, Cronemberger C, Mass T, Genin A (2013) Modelling Growth and Form of the Scleractinian Coral Pocillopora verrucosa and the Influence of Hydrodynamics. PLoS Comput Biol 9(1): e1002849. doi:10.1371/journal.pcbi.1002849

[5] Bourke, P. (2014, September). *DLA - Diffusion Limited Aggregation.* `http://paulbourke.net/fractals/dla/`

[6] T.C. Hasley (November 2000), *Diffusion-Limited Aggregation: a model for pattern formation*, Physics Today.

[7] Salsa, S. *Partial Differential Equations in Action: From Modelling to Theory*, Springer

[8] Chen Xinfu, Hong Jiaxin, Yi Fahuai (1996) Existence, uniqueness and regularity of classical solutions of the mullins-sekerka problem, Communications in Partial Differential Equations, 21:11-12, 1705-1727, DOI: 10.1080/03605309608821243

[9] X. Chen, The Hele-Shaw problem and area-preserving curve-shorting motions, Arch. Rational Mech. Anal. 123 (1993) 117-151.